

Forbidden trajectories for path integrals

Janusz E. Jacak 

*Department of Quantum Technologies, Wrocław University of Science and Technology,
Wybrzeże Wyspiańskiego 27, 50-370 Wrocław, Poland*

 (Received 27 September 2022; accepted 21 February 2023; published 10 March 2023)

The problem of the availability of trajectories for the Feynman path integral is considered. Forbidden trajectories for single-particle integrals are featured in the case of quantum tunneling across barriers. In the case of multiparticle systems of indistinguishable identical particles, some limits for the availability of cyclotron braid trajectories are demonstrated, which leads to the explanation of statistics and correlation in quantum Hall systems of interacting 2D electrons. The homotopy-type restrictions for trajectories close to general-relativity singularities are discussed with indication of quantum properties of black holes manifesting themselves at quasar luminosity or at neutron star merger collapses. The related supplementation to conventional models of accretion disk luminosity in the close vicinity of the event horizon of a supermassive black hole is proposed and compared with observations.

DOI: [10.1103/PhysRevA.107.032207](https://doi.org/10.1103/PhysRevA.107.032207)

I. INTRODUCTION

The Feynman path integral, originally defined for a single particle [1], gives the evolution operator matrix element in the position representation $\langle z_1 | e^{i \int_{t_1}^{t_2} dt \hat{H}(t)/\hbar} | z_2 \rangle$, expressed by the functional integral [2], $I(z_1, t_1; z_2, t_2) = \int d\lambda e^{iS[\lambda(z_1, t_1; z_2, t_2)]/\hbar}$, where $S[\lambda] = \int_{t_1}^{t_2} \mathcal{L}[\lambda(z_1, t_1; z_2, t_2)] dt$ is the classical action for the trajectory $\lambda(z_1, t_1; z_2, t_2)$ with the initial point in the configuration space z_1 at time instant t_1 and the final point z_2 at t_2 . The action is the time integral of the Lagrangian \mathcal{L} for a selected trajectory and is the functional of trajectories with fixed initial and final conditions. This functional is minimal (extremal) for the real classical trajectory defined by the Euler-Lagrange equation for the extreme of the action functional, leading to the classical Hamilton equations with the Hamilton function \mathcal{H} corresponding to the Hamiltonian \hat{H} . The functional integral $I(z_1, t_1; z_2, t_2)$ is taken over all possible classical trajectories linking points z_1 and z_2 including equally the extremal and all nonextremal ones, and the squared modulus of I gives the probability of quantum transition of the particle between points (z_1, t_1) and (z_2, t_2) . The functional integral I is conventionally called a propagator. The equivalence of quantization by Feynman path integration and of canonical quantization in Hilbert space has been evidenced [1,2] and the functional integration quantization occurs very useful and is widely applied in the field theory and in condensed matter [3].

The path integral quantization is explicitly nonlocal in distinction to the Schrödinger equation. The latter is a differential equation for the wave function at a certain potential, but some global topological constraints must be additionally imposed beyond the Hamiltonian form, which does not display nonlocal topological conditions. For example, for bosonic or fermionic particles the Hamiltonian is the same, and the constraint imposed on the symmetry or antisymmetry of the wave function in position representation is an external

condition. The same holds for choosing commutation or anti-commutation algebra of field operators in second quantization representation. Path integral quantization is, however, more general and allows for explicit inclusion of nonlocal factors, which have roots in topological properties of classical trajectories of particles. The algebraic topology [4,5] can describe properties of classical trajectories in a system, and some related global properties cause quantum effects readable via the path integral, supporting in this way related external conditions needed to be imposed on the equivalent Schrödinger equation.

In the present paper we will demonstrate several examples of topological effects in quantum systems, which are evident in path integral quantization but are not explicit in the Schrödinger equation without additional restrictions. First, we will address an elementary example related to single-particle quantum tunneling.

Next, we will present more complex topological effects related to multiparticle systems of indistinguishable particles, their quantum statistics, and quantum correlations conditioned by particle interaction and governed by the global homotopy properties of corresponding configuration spaces and restrictions imposed onto classical trajectories. The experimental illustration of topological behavior possible to be explicitly studied via path integral quantization will be referred to quantum Hall physics in 2D spaces and to specific behavior of multiparticle systems near gravitational singularity of a black hole, which may have significant high-energy consequences.

In the following section the examples of constraints imposed on trajectories in path integrals are presented. The supporting detailed calculations and additional comments are shifted to Appendixes.

II. WHICH TRAJECTORIES ENTER A PATH INTEGRAL?

In the path integral for a single particle [1],

$$I(z_1, t_1; z_2, t_2) = \int d\lambda e^{i \int_{t_1}^{t_2} \mathcal{L}[\lambda(z_1, t_1; z_2, t_2)]/\hbar}, \quad (1)$$

*janusz.jacak@pwr.edu.pl

the summation over trajectories (integration with the measure $d\lambda$ in the space of trajectories) concerns all accessible classical trajectories linking the initial point z_1 in the configuration space of this particle at time t_1 and the final point z_2 at time instant t_2 . Lagrangian $\mathcal{L} = T - V$, where T is the kinetic energy and V is the potential, integrated over time gives the action $S[\lambda]$, a functional over the domain of trajectories. This functional is minimal (extremal) for classical trajectory defined by the Euler-Lagrange equation, $\frac{d}{dt}(\frac{\partial \mathcal{L}}{\partial \dot{z}}) - \frac{\partial \mathcal{L}}{\partial z} = 0$, according to the least action principle. The family of trajectories contributing to the Feynman path integral includes also arbitrary not extremal paths, but those which are classically accessible for the potential $V(z)$ and for the topology of the configuration space. The contribution to the propagator I of all trajectories with the weight $e^{iS[\lambda]/\hbar}$ reproduces the quantum behavior of the particle, the same as that in the Schrödinger formulation with the Hamiltonian $\hat{H} = -\frac{\hbar^2 \nabla^2}{2m} + V(z)$ (depending on configuration space, z can be appropriate dimensionality vector defining position of the particle) [1]. The quantum Feynman path integral is analogous to the Wiener classical path integral [6] applied to the Brownian motion [2]. In distinction to the well-defined Wiener measure for summation of probabilities [2,6], the summation of complex probability amplitudes in a quantum Feynman integral [1] precludes a proper measure definition [2], and the approach is more heuristic. Commonly accepted is the discretization method for explicit summation over trajectories [1,2]. This method clearly shows which trajectories contribute to the sum, arbitrary continuous piecewise paths of segments being minimal (extremal) for boundary conditions on discrete consecutive internal points (approximated even by straight line sectors, without any loss of generality at an infinitesimal time step of discretization), provided, however, that the real extreme trajectory exists for each segment. This is an important restriction for the discretization procedure, because next the integration over all internal points is performed in limits of piecewise trajectory existence. For quadratic Lagrangians these integrals are of Gaussian type, which attain the analytic form only for infinite limits. However, if the piecewise trajectory cannot be constructed in some coordination space region [due to features of the potential $V(z)$ or topological restrictions imposed] the limits cannot always be infinite. This problem has been noticed by Pauli [2,7] and also earlier for Wiener path integrals for Brownian motion with inaccessible regions [2].

Classical trajectories cannot enter potential barriers of arbitrary height but can be virtually placed in energy region beyond the potential barrier as nonextremal paths for selected classical initial and final conditions, which can be also discretized without any restrictions (note that the discretization produces continuous but nondifferentiable paths, similarly as for the Wiener measure). These trajectories lead to quantum tunneling across the classically inaccessible region expressed by the Feynman path integral, the same tunneling effect as that via the solution of the Schrödinger equation. Nevertheless, in the case of an infinitely high barrier no classical trajectories beyond the barrier exist and the propagator across the barrier is zero [8], which is equivalent to the fact that quantum particles do not tunnel through infinitely high potential barriers and cannot penetrate such infinite vertical potential walls. This

simple example shows that not all trajectories contribute to the Feynman path integrals, but only those which are classically accessible (even piecewise) for a given potential and topological restrictions. In another example, the 1D oscillator potential x^2 is the parabola also of infinite height, which, however, does not restrict the possibility of arbitrary piecewise trajectory construction (as parabola is infinitely wide), contrary to a rectangular infinite well or potentials ranged by vertical asymptotes. Instructive would be also the infinite potential of a Dirac delta type, which despite its infinity allows a nonzero transition across it. This is clear due to the fact that the Dirac delta is not a function but a distribution and at best can be considered as the limit of the series of finite height and width ordinary functions with integer 1, which do not impose restrictions on trajectory existence in a path integral. The limiting Dirac delta is nonzero only in a single point (because of limiting value 1 of the integral it is not a function, however), and this point can be selected as a fixed one of the discretization points, which does not conflict with the existence of trajectories on the left and on the right. Using the property for multiplication for path integral [1, chaps. 2–5] (with integration over the intermediate time), one gets nonzero probability transmission from the left to the right. Despite that the infinite barrier of a finite width also can be considered as a limit of finite height functions, the nonzero width persists in the limit, and twice applying the multiplication property on walls of the barrier we get, however, a multiplicative zero factor from the inside of the barrier (without any accessible trajectories there), which causes the whole propagator to vanish.

The constraint to only accessible trajectories in path integrals has profound consequences, generally of topological character, which cannot be easily noticeable in Schrödinger equation formulation. In the elementary example of vanishing of the wave function at infinite potential barriers, this property is evident in path integral quantization, but in the Schrödinger equation approach it needs a study of limiting behavior of finite height barriers. The more complicated situations can occur in collective multiparticle systems of identical particles, when the restriction to only accessible classical trajectories in path integrals has experimentally verified consequences; such topological effects will be discussed in the following section.

III. PATH INTEGRALS FOR MULTIPARTICLE SYSTEMS OF IDENTICAL INDISTINGUISHABLE PARTICLES

If one considers a N -particle system, then the trajectories contributing to path integrals are N -strand bunches in the multiparticle configuration space. Particles can mutually interact, and their dynamics can be restricted additionally by some external potential or other factors like a magnetic field, which can influence availability of trajectories. Each particle contributes with its individual trajectory to the whole multi-strand classical paths. If particles are distinguishable, then the configuration space of N -particle system is

$$P_N = M^N - \Delta, \quad (2)$$

where M is the space (mathematically, manifold) on which all N particles are located, $M^N = M \times M \times \dots \times M$ is the N -fold product of the space M to account individual

trajectories of all particles, and the space M is accessible for each particle equally. The set Δ is the diagonal subset of M^N with coordinates of at least two particles coinciding. Δ is removed from the coordination space P_N to ensure particle number conservation. In this case classical multiparticle trajectories are the collections of single-particle individual paths restricted by the single-particle potential or a magnetic field and interparticle interaction, avoiding crossing of individual single-particle paths in M in the same moment, as the diagonal subset Δ is removed from the space P_N . This does not cause topological quantum effects beyond those for the single-particle case.

The situation changes, however, if particles are identical and indistinguishable. Quantum indistinguishability of identical particles is not explicitly imprinted in multiparticle Hamiltonian $\hat{H} = \sum_i^N (\frac{-\hbar^2 \nabla_i^2}{2m} + V(z_i)) + \frac{1}{2} \sum_{i,j,i \neq j} U(z_i, z_j)$, and some external constraint must be imposed onto the Schrödinger equation (regarding the symmetry or antisymmetry of a multiparticle wave function as for bosons or fermions, correspondingly). This constraint is of an external character and relates to the notion of indistinguishability of particles against their mutual position swapping expressed by changes of their numeration, which should not cause any physically observable effect. Thus, the square of the wave function module must be assumed not to change at particle exchanges, which admits either a plus or minus sign of the wave function at exchanges of particle coordinate pairs, provided that the double exchange of the particle pair restores the initial situation. This conventional reasoning and the related intuitive definition of particle indistinguishability is, however, misleading for 2D manifolds M and can be applied exclusively to 3D physical space (or for higher dimension manifolds M). For a 2D manifold a double exchange of identical indistinguishable particles is topologically distinct from the neutral operation. This needs more precise consideration of particle indistinguishability.

The rigorous inclusion of the indistinguishability of identical particles must be done in classical topological terms in the definition of the multiparticle configuration space, which for N indistinguishable particles attains the form

$$F_N = (M^N - \Delta)/S_N, \quad (3)$$

with the quotient structure by S_N , the permutation group of N -elements. This displays the immunity of the configuration space against arbitrary swapping of indistinguishable particles expressed by a permutation of their numbering. In other words, points in F_N space are unified if they differ by numbering of particles only (in P_N space such points are different). The space F_N does not have an intuitive geometrical visualization in contrast to P_N . It is counterintuitive to any imagination of the multidimensional configuration space with various distributions of differently numbered particles represented, however, as the single point in F_N . A multiparticle trajectory between point distributions which differ in particle numbering only is thus a closed trajectory loop in F_N space (in P_N is open).

Closed trajectory loops in the space F_N form disjoint classes of closed multistrand continuous trajectories starting from a certain point in F_N and finishing in the same point.

Closed multistrand loops in F_N joining the same positions of N particles distinctly numbered are called braids. These braids are open multistrand trajectories in P_N , but are closed loops in F_N . Closed loops in any topological space (arc-connected) \mathcal{A} can be characterized in a topological sense by the first homotopy group $\pi_1(\mathcal{A})$ of this space [4]. The $\pi_1(\mathcal{A})$ group collects disjoint classes of inequivalent loops, which can be deformed one onto another without cutting within the class but cannot between different classes. The space \mathcal{A} is multiply connected if the $\pi_1(\mathcal{A})$ group is nontrivial. Otherwise, when this group is trivial, i.e., $\pi_1(\mathcal{A}) = \{\varepsilon\}$ (where ε is neutral element in the group), the space \mathcal{A} is simply connected. If the space \mathcal{A} is the multiparticle configuration space of indistinguishable particles, F_N , then $\pi_1(F_N)$ is called the braid group (more precisely, full braid group in distinction to pure braid group $\pi_1(P_N)$). The full braid group is usually nontrivial for $N \geq 2$ (except for some special cases, which will be discussed later), and its form depends strongly on the dimension of the manifold M .

For a 3D manifold M (or of higher dimension) the braid group $\pi_1(F_N) = S_N$ [5,9], i.e., the full braid group, is here always the ordinary finite permutation group with $N!$ elements. However, for 2D manifolds, the related braid groups are infinite and more complicated. For $M = R^2$ (2D plane) the full braid group is the so-called Artin group [9,10], which is an infinite and multicyclic group, i.e., is generated by a finite set of generators. These generators can be chosen as σ_i , for $i = 1, \dots, N - 1$ satisfying the following conditions [9];

$$\begin{aligned} \sigma_i \sigma_{i+1} \sigma_i &= \sigma_{i+1} \sigma_i \sigma_{i+1}, \quad \text{for } 1 \leq i \leq N - 2, \\ \sigma_i \sigma_j &= \sigma_j \sigma_i, \quad \text{for } 1 \leq i, j \leq N - 1, |i - j| \geq 2. \end{aligned} \quad (4)$$

The generators σ_i can be selected as elementary exchanges of positions of the i th particle with the $(i + 1)$ -th one, at arbitrary but fixed numbering of all particles [5,9]; cf. Fig. 1. In the case of the 2D manifold M , $\sigma_i^2 \neq \varepsilon$ contrary to the 3D M , for which $\sigma_i^2 = \varepsilon$. The latter condition makes the full braid group simple in three dimensions and equal to the permutation group S_N , despite that both the permutation and Artin groups are multicyclic generated by σ_i , elementary exchanges of neighbors (at arbitrary though fixed numbering of particles), but with different conditions imposed onto these generators in both cases. Full braid groups allow us a precise definition of exchanges of identical indistinguishable particles on arbitrary manifolds. A particle swapping can be visualized in the space P_N as shown in an example in Fig. 2 and assuming that start and final points (before and after particle swapping) are the same point in F_N ; then such a picture illustrates graphically a braid from F_N . Note that the true braids in P_N must also be closed loops in P_N , as in any π_1 group, and thus must link the same distributions of particles with the same particle numbering. The braids in F_N are not braids in P_N except for braids in F_N linking the initial and final points also with identical numbering, thus $\pi_1(P_N)$ is a subgroup of $\pi_1(F_N)$ [5,9] (Fig. 2).

Braids—elements from the full braid group—have a fundamental significance for the definition of multiparticle trajectories contributing to path integrals for identical indistinguishable particle systems. Open trajectories linking various points in F_N space can be attached at arbitrary point on their way by some closed loop—the braid, which means that

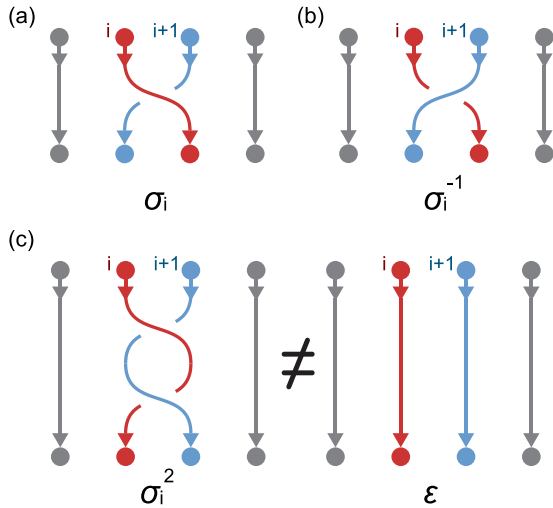


FIG. 1. Braid generators σ_i , $i = 1, \dots, N - 1$ define exchanges of the i th particle with the $(i + 1)$ -th one, while other particles are at rest (at arbitrary but fixed particle numbering). Graphical presentation of σ_i (a) and σ_i^{-1} (b) is depicted. Braids must be closed loops in the space F_N , thus in the illustration the initial and final particle orderings are considered as unified. The braid σ_i^2 (c), though does not change the particle ordering, is not a neutral element in the group ε , unless the manifold M has the dimension >2 .

particles can change their numbering on the way; cf. Fig. 3. The attachment of an arbitrary finite number of braids to various points of the trajectory in F_N is equivalent to the attachment of a single braid, the group product of all added braids. As braids are nonhomotopic, i.e., they cannot be continuously deformed one onto another without cutting, thus the whole space of multiparticle trajectories decomposes into disjoint nonhomotopic sectors. The discontinuity between sectors precludes the definition of the measure $d\lambda$ for the path integral on the whole domain of trajectories. Instead, separate measures can be defined only on disjointed sectors of the domain and the contributions of all sectors must be finally added up with arbitrary unitary weight factors (the unitarity of these weight factors is required to maintain the structure of the

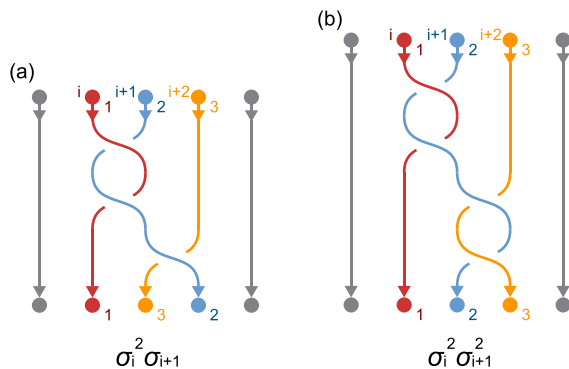


FIG. 2. The full braid group is the group $\pi_1(F_N)$, whereas the group $\pi_1(P_N)$ is called the pure braid group. An ordering of braided particles can change for $\pi_1(F_N)$ (left example), but for $\pi_1(P_N)$ must be conserved (right example). The pure braid group is a subgroup of the full braid group.

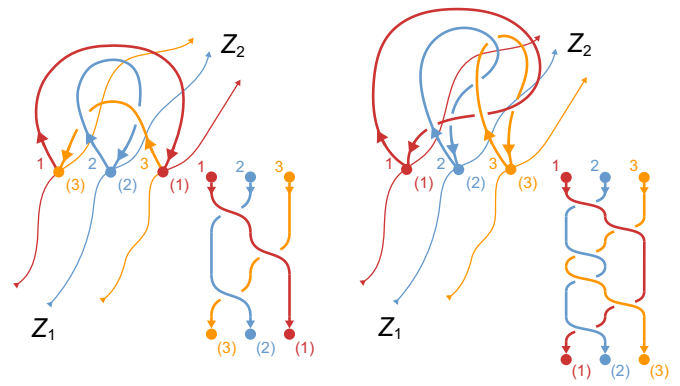


FIG. 3. In F_N space a trajectory linking two different points Z_1 and Z_2 is the multistrand bunch of single-particle paths. The numeration of particles can be varied on the way, i.e., in any intermediate point of the open trajectory an arbitrary braid from $\pi_1(F_N)$ can be attached. In principle, an arbitrary finite number of braids can be attached to multistrand trajectory in various points on the way between initial and final points in F_N ; however, according to the group structure of $\pi_1(F_N)$, the attachment of all these braids is equivalent to the attachment of the group multiplication of all of them, which is also a braid. Braids are nonhomotopic, thus the space of trajectories decomposes into disjointed sectors numbered by various braids. In the illustration different braids are attached to the same 3-strand trajectory in F_3 space. Resulting trajectories cannot be continuously deformed one into another without cutting.

path integral displaying the causality in quantum mechanics [11]). Sectors in the domain of multiparticle trajectories of indistinguishable particles are numbered by braids, thus the weight factors form the unitary scalar representation (1DUR, 1D unitary representation) of the full braid group [5,11,12]. The Feynman path integral for the system of N identical indistinguishable particles attains thus the form

$$I(Z_1, t_1; Z_2, t_2) = \sum_l e^{i\alpha_l} \int d\lambda_l e^{iS[\lambda_l(Z_1, t_1; Z_2, t_2)]/\hbar}, \quad (5)$$

where points $Z_1 = (z_1^1, \dots, z_N^1)$ and $Z_2 = (z_1^2, \dots, z_N^2)$ are two different points in multidimensional configuration space F_N of N indistinguishable particles, which define the start and final points for the propagator $I(Z_1, t_1; Z_2, t_2)$ at time instants t_1 and t_2 , respectively. The discrete index l enumerates braids in the full braid group, and $e^{i\alpha_l}$, $\alpha_l \in [0, 2\pi)$ is the scalar unitary representation of the l th braid (the element of 1DUR of the full braid group). Braid groups are generated by the finite number of generators, and thus are countable or finite and l is a discrete index. The trajectory in F_N , $\lambda_l(Z_1, t_1; Z_2, t_2)$, is the trajectory between Z_1 and Z_2 but with the l th braid attached from the full braid group at some intermediate point of this trajectory. Braids are nonhomotopic, thus the measure in the path space can be only defined separately on each disjointed sector of the path space numbered by l ; such a family of measures for path integration is denoted by $d\lambda_l$.

1DURs of braid groups are precisely defined, though the same braid group can have a variety of distinct 1DURs. Each one defines a different quantization of the same classical system. There are therefore as many different quantum particles

corresponding to the same classical ones as there are different 1DURs of the full braid group for these classical particles.

For 3D manifolds M the full braid group is always S_N [5,9]. There exist only two 1DURs of S_N [5,9], defined on the group generators $\sigma_i \rightarrow \{e^{i0}, e^{i\pi}\}$, leading to bosons and fermions, respectively.

The Artin group [10], the full braid group for $M = R^2$, has, however, an infinite number of 1DURs [9,12–14], $\sigma_i \rightarrow e^{i\alpha}$ with $\alpha \in [0, 2\pi)$ corresponding to so-called anyons [15] (including bosons for $\alpha = 0$ and fermions for $\alpha = \pi$). Note that 1DURs of the Artin group are uniform on its generators, i.e., 1DURs do not depend on the index i of the generator, which follows from the first equation (4). If one takes 1DUR of both sides of this equation, then bearing in mind that scalar representations commute (are Abelian), one obtains $1\text{DUR}(\sigma_i) = 1\text{DUR}(\sigma_{i+1})$, which means independence of $1\text{DUR}(\sigma_i)$ from i .

Exchanges of indistinguishable particles defined by braid groups and their 1DURs display quantum statistics of particles and in the case of anyons are referred to fractional statistics [12,13,15].

The equivalence between path integral quantization and wave function formulation leads to restrictions imposed onto multiparticle wave functions by 1DURs of the related braid group [12,14]. If coordinates of the wave function $\Psi(z_1, \dots, z_N)$ (these coordinates represent classical positions of particles on M) are exchanged in the fashion defined by some selected braid from $\pi_1(F_N)$, then the multiparticle wave function must gain a phase factor equal to 1DUR of this particular braid [14]. This clarifies symmetry or antisymmetry of wave functions for bosons and fermions, and the phase shift $e^{i\alpha}$, $\alpha \in [0, 2\pi)$ at the exchange of a pair of coordinates for anyons.

Despite that the exchange of particles looks like the exchange of two coordinate indices (simple permutation) in the multiparticle wave function $\Psi(z_1, \dots, z_N)$, we must, however, know the braid which actually realizes this exchange in the related configuration space F_N , which essentially depends on the manifold M . Only for 3D manifolds M (and for higher dimensionality) these braids are simple permutations, but for 2D manifolds, not. In the latter case, a simple permutation of coordinate indices in a multiparticle wave function must cause a phase shift of this wave function $e^{i\alpha_i}$, which is the 1DUR of the braid (i th one) actually realizing the exchange of particles in planar geometry prescribed by the simple permutation of coordinate indices. The actual form of this braid (being not the permutation in 2D) and its 1DUR (also different than that of permutation) force the analytic form of the multiparticle wave function to comply with these transformation requirements. Thus, we see that the form of braids, their availability in various physical situations, and their 1DURs are essential for external constraints needed to be imposed on the solution of the multiparticle Schrödinger equation (not fermionic or bosonic, in general), which is equivalent to the explicit role of 1DURs of the braid groups in path integrals given by Eq. (5).

Braid groups depend also on topological factors imposed on multiparticle systems besides the dimensionality of M . A simple example of such factors is an infinitely high potential wall which can occur in some middle place of the manifold M . The system of N particles in this way can be divided into

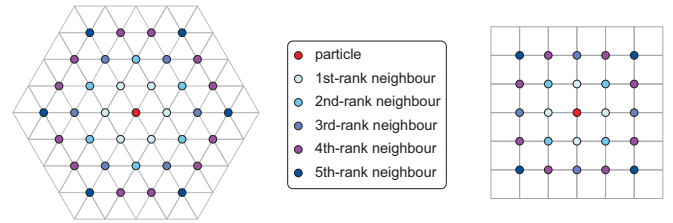


FIG. 4. Two possible classical 2D Wigner lattices: the hexagonal and regular ones. In both lattices the consecutive next-nearest neighbors are marked in different colors. The Bravais elementary cells in both lattices have the same surface size, $\frac{S}{N}$ (because per the elementary cell falls one particle in both lattices), but the hexagonal lattice is more convenient energetically (minimizes the Coulomb interaction).

subsystems $N' + N'' = N$ on both sides of the wall. As any trajectories linking particles form the group N' and N'' are not available, thus the full braid group $\pi_1(F_N)$ cannot be defined as the space F_N starts to be not arc-connected and no quantum statistics can assigned to all N particles simultaneously. Quantum statistics in this case can be assigned separately to subsets of N' and N'' particles. If, however, the wall is of a finite height, then the trajectories linking N' and N'' particles are admissible, and the common statistics of all N particles is restored.

Other examples of forbidden trajectories induced by topological factors can be associated with a magnetic field in 2D systems of interacting particles and for 3D particles in folded spacetime close to gravitational singularity. Both these examples will be presented in the following section.

IV. INACCESSIBLE TRAJECTORIES FOR CHARGED INTERACTING PARTICLES IN TWO DIMENSIONS AT PERPENDICULAR MAGNETIC FIELD PRESENCE

The magnetic field is not a potential one but can restrict trajectories of particles. Charged particles (let us say electrons) in a magnetic field spiral along the field direction, and no other trajectories are attainable at the magnetic field presence for free particles. Braids are classes of homotopic trajectories. Trajectories which belong to the same class can be continuously deformed one into another without cutting, but if they belong to different classes, they are nonhomotopic (cannot be deformed one into another). The braids inside homotopy classes can be, however, restricted by topological factors. In the case of 2D particles, their cyclotron orbits are flat, and therefore of finite size (in 3D not, as the drift along the magnetic field direction is not ranged spatially). They can be deformed, but the availability of deformation can be limited in some special cases. As braids describe exchanges of particle numbering only, thus braids of size of finite cyclotron orbits must fit particle positions. In the 2D gas mutual positions of particles are arbitrary, thus the finite size of planar cyclotron braids does not impose any restriction. However, charged particles (e.g., electrons) repulse themselves and at $T = 0$ K form a uniform classical distribution on 2D positive uniform jellium—the classical 2D Wigner crystal with a hexagonal Bravais lattice or a regular one [16]; cf. Fig. 4. The Bravais lattices minimize the interaction Coulomb energy of

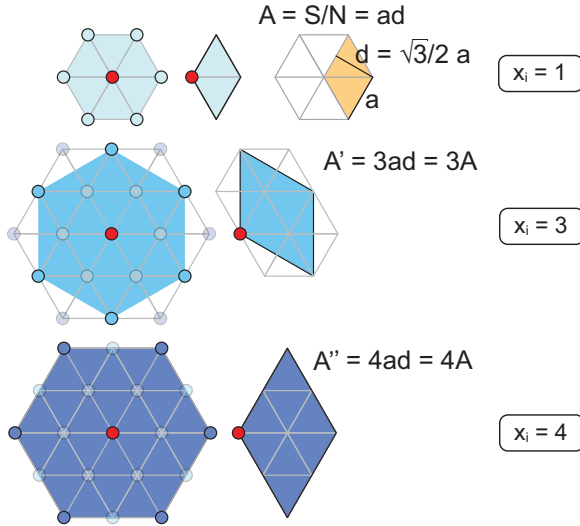


FIG. 5. The Bravais elementary cells for the hexagonal Wigner 2D lattice for nearest, next-nearest, and next-next-nearest neighbors. The sizes of elementary cells for consecutive rank neighbors determine the possible values of x_i , which can enter the commensurability condition (13). Note that the first-rank next-nearest neighbor sublattice contains only $\frac{1}{3}$ of all N electrons, while in the regular lattice (cf. Fig. 6) the first rank next-nearest neighbor sublattice contains $\frac{N}{2}$ electrons.

charged particles (electrons) distributed on positive uniform jellium, which is an electrostatic problem at $T = 0$ K, when the classical kinetic energy is zero. The hexagonal lattice attains the minimal energy. The regular one has slightly greater Coulomb energy (classical kinetic energy in both cases is zero at $T = 0$ K), but allows a convenient regular distribution of next-nearest neighbors (of first rank) including half of all particles, whereas the hexagonal lattice gives only one third of particles as next-nearest neighbors (of first rank), as illustrated in Figs. 5 and 6.

Cyclotron braids, even if deformed, must fit to Wigner crystal distribution of interacting particles in 2D, which can be expressed as the commensurability of cyclotron orbit size (the surface size of orbits) with elementary cells of a Bravais lattice including also Bravais sublattices of next-nearest neighbors of consecutive ranks (here the advantage of a regular lattice manifests itself for next-nearest neighbors of first rank). Otherwise, when cyclotron orbits are not commensurate with particle distribution, neither for nearest neighbors nor for next-nearest neighbors of arbitrary rank, then braid trajectories are inaccessible and the braid group cannot be defined.

The size of classical cyclotron 2D trajectories is defined by the Bohr-Sommerfeld rule. This rule precisely determines the surface field of 1D classical phase space encircled by a classical trajectory. The Bohr-Sommerfeld rule can be applied to components of 2D kinematic momentum of a single electron at a constant perpendicular magnetic field, $P_x = -i\hbar \frac{\partial}{\partial x}$ and $P_y = -i\hbar \frac{\partial}{\partial y} - eBx$ (e is the electron charge), which define the effective 1D phase space, $Y = \frac{P_x}{eB}$ and P_y , because $[Y, P_y]_- = i\hbar$ [independently of magnetic field gauge, though here we used the Landau gauge for concreteness, $\mathbf{A} = (0, Bx, 0)$, $\mathbf{B} = \text{rot}\mathbf{A} = (0, 0, B)$]. The smallest surface in this effective phase

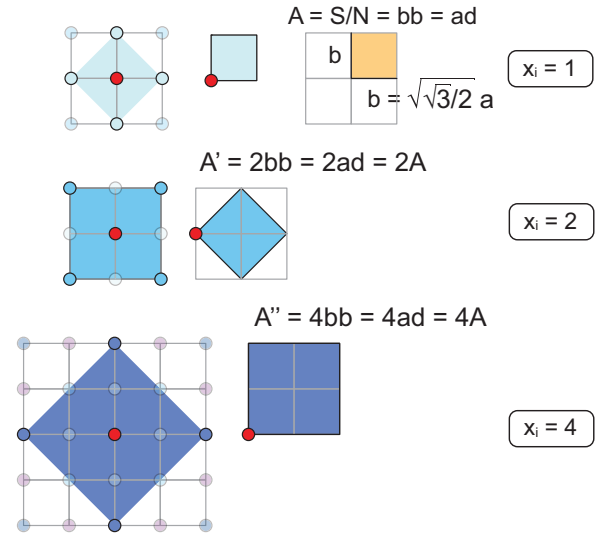


FIG. 6. The Bravais elementary cells for the regular Wigner 2D lattice for nearest, next-nearest, and next-next-nearest neighbors (a is the distance between electrons in hexagonal lattice and d is the height in the triangle as in Fig. 5). The sizes of elementary cells for consecutive rank neighbors determine the possible values of x_i , which can enter the commensurability condition (13).

space (according to the Bohr-Sommerfeld rule) determines the smallest classical cyclotron orbit size, $\frac{\hbar}{eB}$; it is the surface of the quantum of magnetic flux $\frac{h}{e}$ conserved despite any deformation, $h = 2\pi\hbar$ (details are shifted to Appendix A). This invariant surface size of the 2D cyclotron orbit plays the role of a topological factor limiting braid groups and their 1DURs.

For magnetic field sufficiently large that the gap between Landau levels (LLs), proportional to the magnetic field, is much larger than Coulomb interaction between electrons, one can consider separately electrons filling consecutive LLs in a multiparticle system with the size of cyclotron orbits $(2n + 1)\frac{\hbar}{eB}$, where n is the Landau index (cf. Appendix A). Moreover, one can distinguish between two opposite spin orientations of electrons as the Zeeman splitting is of the order of the gap between LLs, and opposite spin electron subsystems can be considered separately. Spin orientation does not influence the cyclotron orbit size and does not change homotopy of trajectories. Due to the indistinguishability of electrons, cyclotron braids must be consistent with LLs structure and magnetic field flux quantization. This consistency expresses itself via the commensurability condition of cyclotron orbit size and surface of classical Wigner crystal Bravais cells including sublattices of next-nearest neighbors of consecutive ranks, which ensures possibility of the exchanging of interacting 2D electrons. Such a commensurability condition is the homotopy invariant for a particular LL. Note that LL structure and related size of cyclotron orbits are single-particle properties (Landau quantization of a single 2D electron in a perpendicular magnetic field). Such a prequantization has been justified for path integration quantization of a single particle in a magnetic field via the equivalence to geometrical quantization [17,18]. As we aim to consider quantum statistics and correlations in a multielectron system in a magnetic

field, we adopt the similar concept of prequantization of the single particle. This allows for the identification of homotopy invariants separately for particular LLs including spin.

The commensurability condition of a Wigner crystal elementary cell (existing only for interacting particles) with cyclotron orbits (or braids) is a multiparticle property. For a fixed number of electrons N per surface S of the sample and the rigidly defined surface size of cyclotron orbits in particular LLs (via the Bohr-Sommerfeld constraint imposed on surface of the classical orbit; cf. Appendix A) one can get all admissible LL filling rates $\nu = \frac{N}{N_0}$ ($N_0 = \frac{BS_e}{h}$ is the degeneracy of LLs, a single-particle property) via the commensurability condition for braids in the classical Wigner lattice of these electrons. This reproduces the hierarchy of the quantum Hall effect observed experimentally, including integer (IQHE, integer quantum Hall effect [19]) and fractional (FQHE, fractional quantum Hall effect [20]).

The simplest commensurability condition for electrons in the lowest LL (LLL) with spin orientation along the magnetic field has the form

$$\frac{S}{N} = \frac{h}{eB}, \quad (6)$$

which means that the size of the elementary cell in a Bravais lattice of a classical Wigner crystal, $\frac{S}{N}$, perfectly fits the surface size of a single-loop cyclotron orbit of electrons in the LLL, i.e., the quantum of magnetic field flux $\frac{h}{e}$ divided by the magnetic field B (in the above equation S is the sample surface and N is the number of indistinguishable electrons). In this case the braids, which must be half of cyclotron loops [21], can exchange the closest neighboring electrons. The commensurability condition (6) is a homotopy invariant; it is robust against braid deformations, i.e., it confines topologically the homotopy of trajectories. If one takes into account that the degeneracy of Landau levels is $N_0 = \frac{BS_e}{h}$, the equation (6) can be rewritten as $\frac{N}{N_0} = 1$. Thus we see that the cyclotron commensurability condition (6) occurs at the completely filled LLL, i.e., at filling factor $\nu = \frac{N}{N_0} = 1$. However, this is not only complete filling of this level (which would happen even in the noninteracting gas), but (6) expresses the strong correlations in the interacting planar system of electrons, for which a Wigner crystal can be defined. The wave function corresponding to this correlated state must transform at coordinate exchanges as 1DUR of the full braid group (the Artin group in this case). Assuming original electrons to be fermions, this 1DUR is $\sigma_i \rightarrow e^{i\pi}$. As the multiparticle wave function in the lowest Landau level must be an analytical function [22], thus the only possible form of this function is

$$\Psi_{\nu=1}(z_1, \dots, z_N) = \mathcal{A} \prod_{i>j}^N (z_i - z_j) e^{-\sum_i^N |z_i|^2/4l_B^2}, \quad (7)$$

where \mathcal{A} is the normalization constant, $l_B = \sqrt{\frac{h}{eB}}$ is the magnetic length, and the envelope function $e^{-\sum_i^N |z_i|^2/4l_B^2}$ is the interaction independent factor for any multiparticle wave function in the LLL [because the single-particle state in the LLL at cylindrical gauge of magnetic field is $f(z)e^{-|z|^2/4l_B^2}$, where $f(z)$ is an arbitrary analytic function [22], which can be chosen as $\sim z^n$, $n = 0, \dots, N_0 - 1$ displaying Landau level

degeneracy]. The polynomial part of the wave function (7) is uniquely derived from 1DUR of the full braid group in the interacting system. The 1DUR, $\sigma_i \rightarrow e^{i\pi}$ forces the monomial $(z_i - z_{i+1})$ in the wave function, because the exchange of the i th particle with the $(i+1)$ -th one is the rotation on the complex plane of the complex number $z_i - z_{i+1}$ by the angle π , which must produce in the wave function the phase shift $e^{i\pi}$, just as the monomial $z_i - z_{i+1}$. This reasoning can be generalized onto $(z_i - z_j)$, as the exchange of the i th particle with the arbitrary j th one is realized by the braid $\sigma_i \sigma_{i+1} \dots \sigma_{j-1} \dots \sigma_{i+1}^{-1} \sigma_i^{-1}$, which has also 1DUR $e^{i\pi}$.

One can notice that the polynomial in Eq. (7) is just the Vandermonde determinant of the Slater function of $N = N_0$ noninteracting fermions in the LLL [the envelope part is the same as in (7)],

$$\begin{vmatrix} 1, z_1, \dots, z_1^{N_0-1} \\ 1, z_2, \dots, z_2^{N_0-1} \\ \dots \\ 1, z_N, \dots, z_N^{N_0-1} \end{vmatrix} = \prod_{i>j}^N (z_i - z_j). \quad (8)$$

Due to (8) we see that the same multiparticle wave function (7) is the ground state of interacting particles (here electrons), i.e., for a strongly correlated state at $\nu = 1$ corresponding to IQHE, and, on the other hand, is the ground state of the gaseous system of noninteracting particles at $\nu = 1$, which is not the IQHE state. The energies of this same state in the Hilbert space are different in both these cases, as they correspond to two different Hamiltonians,

$$\begin{aligned} \hat{H}_1 &= \sum_{i=1}^N \frac{(-i\hbar\nabla_i - e\mathbf{A}_i)^2}{2m} + \sum_{i,j,i>j}^N \frac{e^2}{4\pi\epsilon\epsilon_0|\mathbf{r}_i - \mathbf{r}_j|} \\ &+ \frac{\rho_0^2}{2} \int_S d^2r \int_S d^2r' \frac{e^2}{4\pi\epsilon\epsilon_0|\mathbf{r} - \mathbf{r}'|} \\ &- \rho_0 \sum_{i=1}^N \int_S d^2r \frac{e^2}{4\pi\epsilon\epsilon_0|\mathbf{r} - \mathbf{r}_i|}, \end{aligned} \quad (9)$$

for an interacting electron system, and

$$\hat{H}_2 = \sum_{i=1}^N \frac{(-i\hbar\nabla_i - e\mathbf{A}_i)^2}{2m}, \quad (10)$$

for gaseous noncorrelated particles. In (9) the first term is the kinetic energy [the same as in (10)], and the next three terms describe electron-electron, jellium-jellium, and electron-jellium interactions, respectively. In above formulas, \mathbf{A}_i is the vector potential of magnetic field B for i th electron; it is convenient to choose it in symmetric gauge, $\mathbf{A}_i = \frac{1}{2}(-By_i, Bx_i, 0)$ for circular geometry of the sample with the surface S ; $\rho_0 = \frac{N}{S}$ is the uniform charge density of the jellium, and ϵ_0 and ϵ are dielectric constant and material permittivity, respectively. For a correlated state of the system described by the Hamiltonian (9) the energy is negative counted from the bottom of the LLL and depends on N (can be calculated; cf., e.g., Refs. [23,24]), whereas for the gaseous system it is zero (in the same scale) and particle independent. The lowering of the energy due to correlations (6) of interacting electrons is small and stabilizes this state only if this energy

gain is not washed out by the temperature chaos $k_B T$ (k_B is the Boltzmann constant). Thus IQHE is observable at extremely low temperatures of the scale of the energy gain due to correlations, much lower than the gap between LLs. The “accidental” coincidence of the multiparticle wave function for the correlated state (7) with the gaseous Slater determinant for a completely filled lowest Landau level in a gaseous system follows from the same full braid group for the gas and for the correlations due to interaction (6) occurring at complete filling of the LLL.

However, if the LLL is fractionally filled ($N < N_0$), then such a coincidence disappears and the multiparticle wave functions for interacting electrons are different than those for noninteracting gaseous particles. For interacting electrons the pattern of braid correlation changes, and the corresponding wave function is governed by the 1DUR of a different braid group associated with different correlations. In the gaseous system no correlations exist (as the Wigner crystal does not exist without interaction) except for fermionic (for electrons) representation of full braid group of gaseous system, which results in the Slater function for arbitrary filling rate $\nu < 1$ (with the degeneracy $\binom{N_0}{N}$, the number of combinations of N elements from N_0). The wave function of interacting N electrons is, however, different. In general, it is a linear combination of all $\binom{N_0}{N}$ degenerated states of a gas, which span the appropriate subspace in the Hilbert space. For some specific filling fractions the multiparticle states will be correlated states with lower energy (the energy gain due to correlations for Hamiltonian (9)), provided that for this filling rate some commensurability of the cyclotron orbit with a Wigner crystal is admitted. These specific filling rates create the so-called hierarchy of FQHE [21] and are observed experimentally [20,25].

An example of such a situation is the state at fractional filling $\nu = \frac{1}{q}$ (q odd integer) of the LLL described by the multiparticle Laughlin wave function [26]. To identify theoretically other filling rates for correlated states (FQHE states) many various approaches have been proposed, like the Haldane-Halperin model [27,28] of daughter states of consecutive anyon generations (anyons are associated with quasiparticles or quasiholes for the Laughlin state [26]), the composite fermion (CF) model of hypothetical quasiparticles created from electrons and pinned to them auxiliary fictitious magnetic field quanta [29], or the Halperin model of multi-component Laughlin states [30]. The anyonic model [27,28] has been abandoned early, as the size of daughter wave functions quickly exceeds the sample size, and the CF fermion model partly elucidates the FQHE hierarchy in the LLL, but not of so-called enigmatic states in the LLL and fails in higher LLs. Moreover, the trial wave functions in the CF model [31] do not keep the required symmetry and can be treated as only variational functions. The Halperin multicomponent model perfectly agrees with energy gain (from experiment and from numerical simulation of toy systems) for some chosen correlated states, but is unable to predict in advance which states it concerns.

In order to account for all LL filling rates at which the FQHE correlations occur one must consider available cyclotron braid trajectories for interacting electrons in two

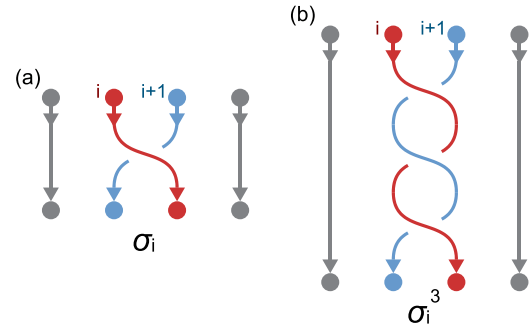


FIG. 7. The braid σ_i^{2k+1} with additional k loops is also the exchange of the i th particle with the $(i + 1)$ -th one, in the illustration for $k = 1$ (right). In the case when σ_i cannot be implemented as being too short, the braids σ_i^{2k+1} , $i = 1, \dots, N - 1$ take the role of braid group generators (in the simplest case σ_i^3). They generate a cyclotron braid subgroup.

dimensions. To be more specific, let us consider a larger magnetic field than that B at which IQHE occurred, let us say $3B$, at which the size of the single-loop cyclotron orbit in the LLL is $\frac{h}{e3B}$ and is far too small to match even nearest neighbors in the Wigner crystal lattice, $\frac{h}{e3B} < \frac{S}{N}$ [if compared to (6) for the same S and N]. Such short cyclotron braids (with the size of single-loop cyclotron orbits) are thus inaccessible, i.e., the simplest exchange braids σ_i cannot be defined for electrons in the LLL at the field $3B$. Nevertheless, some other braids (also exchanges of nearest neighbors; cf. Fig. 7), σ_i^3 , $i = 1, \dots, N - 1$ can be of a larger size (cf. Appendix A) sufficient to match nearest electrons in the Wigner lattice. The braids σ_i^3 , $i = 1, \dots, N - 1$ (more generally, σ_i^{2k+1}) can generate the new braid group: the subgroup of the initial full braid group and called a cyclotron braid subgroup. This is related to the fact that the multiloop cyclotron trajectory in the LLL has a larger size than the single-loop one in the case when single-loop cyclotron orbits, and braids built of their pieces are too short and cannot match even nearest particles (cf. Appendix A). The multiloop cyclotron orbit with $2k + 1$ loops (k integer) has the size $\frac{(2k+1)h}{eB}$ in the LLL in the case when too small single-loop orbits cannot define braids σ_i . The related new elementary braids, half of the multiloop cyclotron orbits, σ_i^{2k+1} , are the exchanges of closest electrons with additional k loops (in the example, for field $3B$, $k = 1$). The proof of this fact follows from the Bohr-Sommerfeld constraint imposed on orbits in multiply connected space [32]. This proof is briefly presented in Appendix A, and it displays the essential difference between σ_i^{2k+1} in two situations: in the case when σ_i can be implemented, then the braid σ_i^{2k+1} is simply $(2k + 1)$ times repeating σ_i (and σ_i^{2k+1} is of the same size as σ_i in this case); however, when σ_i cannot be implemented as it is too short (is the forbidden trajectory), the braid σ_i^{2k+1} is not multiple exchange, as σ_i does not exist. In the latter case σ_i^{2k+1} ($i = 1, \dots, N - 1$) take the role of the elementary exchanges of closest neighboring electrons, the i th with the $(i + 1)$ -th one, and have a larger size.

The braid subgroup generated by σ_i^{2k+1} (called the cyclotron braid subgroup [21]) has different 1DURs than the full braid group, and these new 1DURs decide on braid symmetry

and the shape of the corresponding multiparticle wave function. For an exemplary 3B magnetic field, the multiparticle wave function attains the form of the Laughlin function,

$$\Psi_{\nu=1/3}(z_1, \dots, z_N) = \mathcal{B} \prod_{i>j}^N (z_i - z_j)^3 e^{-\sum_i^N |z_i|^2 / 4l_B^2}, \quad (11)$$

and the filling fraction is $1/3$ (because degeneracy of LLs grows linearly with magnetic field and gives $\nu = \frac{N}{N_0} = \frac{1}{3}$ for 3B).

The detailed mathematically rigorous derivation of the Laughlin function is presented in Ref. [33]. In short, when the full braid group had the 1DUR $\sigma_i \rightarrow e^{i\alpha}$, then the projective 1DUR for the cyclotron subgroup must be $\sigma_i^{2k+1} \rightarrow e^{i(2k+1)\alpha}$ (for original fermionic electrons one must choose $\alpha = \pi$). This projective 1DUR defines the symmetry of the polynomial part of the multiparticle wave function of interacting 2D electrons at field $(2k+1)B$ (in the simplest case, 3B). This polynomial must be of the form of a Jastrow polynomial $\prod_{i>j}^N (z_i - z_j)^{2k+1}$ as in the Laughlin function (11), because the monomial $(z_i - z_j)^{2k+1}$ is induced by the 1DUR of the braid σ_i^{2k+1} (i.e., $\sigma_i^{2k+1} \rightarrow e^{i(2k+1)\pi}$) at the rotation of the complex number $(z_i - z_j)$ by the angle π (exchange of x_i with x_j coordinates of the multiparticle wave function). Thus this monomial must be of the form $(z_i - z_j)^3$ (for $k = 1$) as 1DUR(σ_i^3) = $e^{3\pi}$.

The cyclotron subgroup (when inaccessible braids σ_i are removed from the braid group) describes simultaneously the new commensurability condition (new correlation pattern, new homotopy invariant),

$$\frac{(2k+1)h}{eB} = \frac{S}{N}. \quad (12)$$

For example, for $k = 1$ the condition (12) is satisfied at 3B [cf. Eq. (6)], for which the degeneracy of the LLL equals $N_0 = \frac{3BSe}{h}$ and $\nu = \frac{N}{N_0} = \frac{1}{3}$; this is the most pronounced manifestation of FQHE. The generalization to other k is evident and leads to the derivation of Laughlin functions for $\nu = \frac{1}{q}$, $q = 2k + 1$ [33].

In the case when the q -loop cyclotron orbit does not fit the nearest neighbors in the Wigner lattice, one can consider the commensurability of each loop separately taking into account also next-nearest neighbors in the Wigner lattice. In this way one can define the general commensurability condition [21],

$$\frac{SB}{N} = \frac{h}{x_1 e} \pm \frac{h}{x_2 e} \pm \dots \pm \frac{h}{x_q e}, \quad (13)$$

which gives the most general filling fraction for various phases of FQHE in the LLL, i.e., the complete FQHE hierarchy in the LLL,

$$\nu = \frac{N}{N_0} = \left(\frac{1}{x_1} \pm \frac{1}{x_2} \pm \dots \pm \frac{1}{x_q} \right)^{-1}, \quad (14)$$

where $N_0 = \frac{BSe}{h}$ is the degeneracy of LLs (the single-particle property). In the above formulas the particular $x_i = 1, 2, 3, \dots$, ($i = 1, \dots, q$, $q = 2k + 1$) is the ratio of all electrons to next-next nearest neighbors in the Wigner lattice; for consecutive ranks of next-nearest neighbors each of x_i can attain independently of i the values 1 (for nearest neighbors

in hexagonal lattice), 2 (for first rank next-nearest neighbors in regular lattice), 3 (for first rank next-nearest neighbors in hexagonal lattice), 4 (for second rank next-nearest neighbors in hexagonal lattice), and so on (cf. Figs. 5 and 6). The \pm between components in (13) and (14) display two possible circulations of consecutive loops in the $q = 2k + 1$ -loop cyclotron orbit, congruent or inverse (in the shape of an eight, in the latter case). The FQHE hierarchy (14) perfectly fits experimental data in GaAs and graphene [25,33–37]. For $x_1 = \dots = x_q = 1$ (and $+$ instead of all \pm) one gets $\nu = \frac{1}{q}$ as for Laughlin functions [26], x_i larger than 1 define subsets of differently correlated electrons in a similar manner as in the Halperin multicomponent state [30]. The specific choice, $x_1 = \dots = x_{q-1} = 1$ and $x_q = y \geq 1$ (and \pm before only the last term) gives the CF hierarchy [29], $\nu = \frac{1}{(q-1)y \pm 1}$. More than single x_i larger than 1 describe the so-called enigmatic FQHE states in the LLL that is inaccessible for CF model [21].

Various forms of the cyclotron braid subgroup conditioned by the availability of specific cyclotron braids corresponding to the general commensurability pattern (13) explain the origin of FQHE hierarchy and elucidate former partial heuristic models, like Halperin multicomponent generalization of the Laughlin function [30] or CF model [29]. In Halperin theory [30] the trial wave function in the form of the multicomponent Laughlin function for the electron system variationally divided into subsystems corresponds actually to subsets of next-nearest neighbors of various rank in the electron Wigner lattice commensurate with selected loops of multiloop orbit as given in (13). This condition defines precisely the related generators of the cyclotron subgroups and also uniquely shapes (via 1DURs of particular cyclotron braid subgroups) the multiparticle wave functions [21], as briefly summarized in Appendix B. The subsets of electrons creating sublattices of particular rank of next-nearest neighbors in the Wigner crystal are just those subsets of electrons featured in the Halperin multicomponent wave functions [30]. In the CF model the Jain's hierarchy $\nu = \frac{1}{(q-1)y \pm 1}$ [29] is the subcase of (14) for a specific choice $x_1 = x_2 = \dots = x_{q-1} = 1$ and $x_q = y$ (and last \pm maintained). Only in this case the multiloop cyclotron orbit structure can be imitated by fictitious auxiliary field flux quanta ($q - 1$ of them) attached to electrons in the CF model. Jain suggested further [29] that his parameter y is the Landau index in the model artificial system of noninteracting spinless fermions in a resultant magnetic field reduced by an average field of fluxes pinned to electrons. This is, however, confusing, as actually $y = x_q$ and is linked to the rate of next-nearest neighbors in Wigner lattice, x_q . This integer, similarly as the other x_i in Eq. (13), equals $\frac{N}{N'}$ where N' is the number of next-nearest neighbors of some rank in the Wigner lattice of N electrons. This mixing of the sense of the integer y causes in the CF model the next error: the CF wave function is artificially assumed in the form of a gaseous function in y th completely filled LL in Jain's model system of spinless gaseous fermions and projected onto the LLL (to remove poles existing in gaseous functions in higher LLs but precluded in the LLL also for interacting electrons). Such a trial CF wave function has a correct rank of the polynomial part (for $y = 1, 2, 3, 4$) because y th spinless LL is filled with $\frac{N}{y}$ electrons (similar to the number of next-nearest neighbors for

$x_q = y$), but it does not keep the braid symmetry exhibited by exact multielectron wave functions (as given in Appendix B). Thus the CF trial wave functions can be treated as the variational wave functions only (the variational degree of freedom corresponds here to the arbitrariness in the definition of the projection onto the LLL from higher LLs in CF construction). The proper-symmetry wave functions for hierarchy (14) are presented in [21] (cf. Appendix B).

We see thus that FQHE is the result of changing the accessibility of cyclotron braid trajectories when the magnetic field varies. The same occurs for FQHE in higher LLs, which agrees with the FQHE observation in higher LLs [38] in GaAs and in graphene, including bilayer graphene [34,39]. Discussion of cyclotron orbits and related braids availability explains all up-to-date observed features related to FQHE in GaAs 2DES in the graphene monolayer and bilayer and also in fractional Chern topological insulators without any magnetic field (substituted, however, by the Berry field). This is visualized both in the shape of multiparticle wave functions and, equivalently, in quantum statistics (and correlations) described in the framework of path integral quantization. The universal aspect of similar FQHE manifestations in different materials, like GaAs 2DES, the graphene monolayer or bilayer, and Chern topological insulators, is linked with the forbidden braid trajectories in varying homotopy classes of trajectories in response to a similar topological factor (magnetic field or Berry field).

The results presented in this paragraph and related to FQHE are invoked here in order to demonstrate the experimentally verifiable effects of inaccessibility of some trajectories in path integrals. They were formerly presented in even more issues for a variety of materials used in Hall experiments (GaAs and graphene, for both single layers and double layers). It is interesting to mention an experiment which allows the observation of the homotopy change of trajectories by a macroscopic factor on demand—a vertical electric field applied to a double-layer Hall system (bilayer graphene in this experiment [40]), which on demand can block hopping of carriers between layers in one way along the electrical field. This, however, completely precludes hopping of closed multiloop trajectory between layers (all loops must be placed thus in a single layer, but without the electrical field, loops can be shared between both layers), and the effect is visible in the experiment as the change of FQHE hierarchy upon switching on and off this electrical field (the experiment is simple as the voltage required is of order of 1 V [40]).

V. HOMOTOPY OF TRAJECTORIES CLOSE TO GENERAL-RELATIVISTIC GRAVITATIONAL SINGULARITY

Let us now consider constraints imposed onto classical trajectories close to the gravitational singularity associated with the notion of a black hole. The related folded spacetime can be described in terms of general-relativistic metric satisfying the Einstein equations for gravitation. The Schwarzschild metric [41] is the solution of general-relativistic Einstein equations for a spherical nonrotating and uncharged body with

the mass M ,

$$-c^2 d\tau^2 = -\left(1 - \frac{r_s}{r}\right)c^2 dt^2 + \left(1 - \frac{r_s}{r}\right)^{-1} dr^2 + r^2(d\theta^2 + \sin^2\theta d\phi^2), \quad (15)$$

where τ is the proper time, t is the time measured infinitely far from the massive body, r, ϕ, θ are rigid spherical coordinates, the same as for a remote observer, and $r_s = \frac{2GM}{c^2}$ is the Schwarzschild radius defining the event horizon (G is the gravitation constant, c is the light velocity in the vacuum). Equation (15) defines the curved spacetime for $r > R$, where R is the radius of a central body and for $R = 0$ is addressed to a black hole without charge and angular momentum. The Schwarzschild metric has a singularity at $r = 0$, which is an intrinsic curvature singularity surrounded by the event horizon sphere with the radius r_s , the region from which neither matter nor light can escape. The Schwarzschild metric has also a singularity on the event horizon $r = r_s$, because of the second term in Eq. (15). This singularity is, however, apparent (called a coordinate singularity) and disappears when changing to other coordinates. The metric (15) is, however, defined only on the exterior region $r > r_s$ or on the interior region $r < r_s$; in the latter region, the timelike intervals became spacelike and conversely. This is also an artificial property related to specific choice of coordinates; in this case, the choice of ordinary spacetime coordinates is the same as of a remote observer. If, however, one changes to another coordinate system corresponding to a different slicing of the same folded spacetime onto its spatial and time parts, the ostensible singularity at the event horizon disappears, but the horizon is still and universally defined as the boundary surface of an area close to the central singularity from which any matter or light cannot escape. In the metric (15) a remote observer can notice the matter falling onto event horizon of the black hole infinitely long, i.e., the falling matter achieves the event horizon at $t \rightarrow \infty$ and it never crosses the horizon for this observer. If one changes to other coordinates, e.g., using proper time instead of t , the matter can smoothly pass the event horizon within a finite period of the proper time and then also within a finite period of the proper time any motion terminates in the central singularity. This has been demonstrated in various coordinates in metrics proposed by Lemaitre, Eddington-Finkelstein, Kruskal-Szekeres, Novikov, or Gullstrand-Painlevé [42–44]. Each of these specific metrics displays a different slicing of the same curved spacetime into space and time its components, with emphasizing of the Kruskal-Szekeres metric, being the maximally extended solution of the Einstein equations (analytic in the whole accessible domain) [43,44]. However, there does not exist a rigid time-independent space coordinate system describing simultaneously the outer and inner regions with respect to r_s . Hence, the stationary metric (15), the Schwarzschild metric, describes the falling of matter on the event horizon in infinite time in ordinary coordinates of a remote observer. In this metric, the spatial inner volume below the event horizon is zero, though in nonstationary coordinates it is nonzero [42–44] and particles pass the event horizon and terminate their motion in central singularity within a finite period of the proper time.

The outer vicinity of the event horizon, $r > r_s$, is well described by (15) in the stationary system of coordinates (t, r, θ, ϕ) , the same as for a remote observer. In this region one can thus use the same path integral (1) or (5), without having to modify the coordinates of position and time. This convenient opportunity allows for the easy study of trajectories expressed in ordinary rigid and stationary coordinates and to observe the change of the homotopy of these trajectories as they approach the event horizon. In this case a topological factor which precludes availability of trajectories except for spirals with single cross-points is the curvature of gravitationally folded spacetime close to the singularity, as will be demonstrated below.

The qualitative change of the trajectory homotopy takes place at the so-called photon sphere rim at the distance from the central singularity $1.5r_s$, i.e., $0.5r_s$ beyond the horizon. The photon sphere rim in the metric (15) is defined by the innermost unstable circular orbit for any particle, even massless. Any particle, massive or massless, unavoidably spirals onto the event horizon if it passes the photon sphere rim in an inward direction. Beneath the photon sphere rim no circular orbits are possible. This is quite different in comparison to the Newton gravitation center, for which circular orbits are available at an arbitrary small distance from the pointlike gravitation center. For a Newton gravitation center various conic section trajectories are accessible for particles arbitrarily close to the center. Even though for a large distance from the gravitation center the Schwarzschild trajectories can be approximated by conic sections (slightly modified with some additional precession of elliptical orbits, like that observed for Mercury in the Sun's gravitation), in proximity of the event horizon the difference in accessible trajectories is essential. Conic sections allow formation of closed arbitrarily small local loops from pieces of various trajectories because conic sections can cross in two points (like a circle with ellipse, hyperbole, or parabola). This is in contrast to spirals below the innermost unstable circular orbit, where accessible spirals can intersect in a single point only. Outside the photon sphere the situation changes and closed trajectories are possible because deformed conic sections are admissible here. The innermost unstable circular orbit (the photon sphere rim) separates two different space regions with different classes of homotopy of trajectories. The proof of the above is presented in Appendix C.

An exchange of two particle positions in some manifold requires the existence of two oppositely directed different trajectory sectors joining these points, which together form a local closed loop in this manifold. The absence of such closed trajectory loops for particles beneath the photon sphere rim precludes the possibility of mutual interchanges of particle positions in systems of N identical indistinguishable particles located on some manifold $M^* \subset \tilde{R}^3$ [\tilde{R}^3 is the 3D position space R^3 folded according to the metric (15)], and M^* is the subset of the rotationally symmetrical region with $r \in (r_s, 1.5r_s)$. Particles located in M^* have admissible trajectories exclusively in the form of short spirals directed onto the event horizon. No other trajectories are possible here. It is unreachable to form a closed loop from pieces of these spirals, as different spirals defined by Eqs (C5) and (C6) can intersect only in a single point (in contrast to conic-section-like

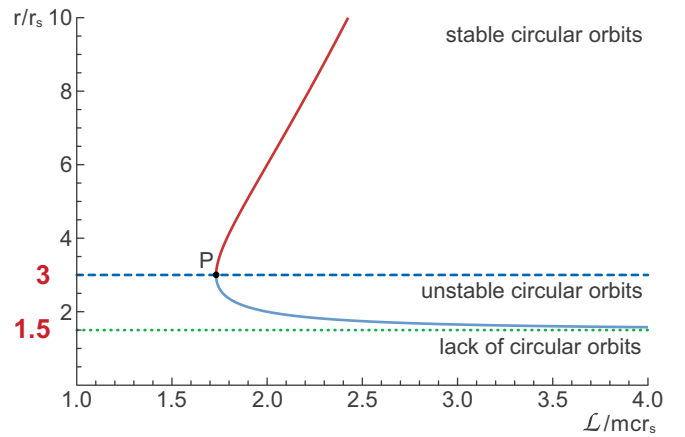


FIG. 8. Radii of stable (red) and unstable (blue) circular orbits in Schwarzschild geometry. The innermost circular stable orbit occurs at $r = 3r_s$ (point P on the level of dashed line in blue color), whereas the innermost unstable circular orbit occurs at $r = 1.5r_s$ (asymptotic dotted line in green color). Below $r = 1.5r_s$ no circular orbits exist.

trajectories); cf. Eq. (C6) in Appendix C with the integral in limits $r \in (r_s, 1.5r_s)$. The homotopy type of trajectories cannot be changed by local interaction, and trajectories for particle exchanges are not available here also for interacting particles. The topological constraint induced by the space curvature in folded spacetime close to the gravitational singularity essentially limits the availability for trajectories. If on a manifold $M^* N$ identical indistinguishable particles are located, then the multiparticle configuration space of these particles, $F_N = (M^{*N} - \Delta)/S_N$, becomes simply connected, whereas for any M beyond the sphere $r = 1.5r_s$, $F_N = (M^N - \Delta)/S_N$ is multiply connected.

For a simply connected space the first homotopy group of this space is trivial, while for multiply connected it is nontrivial [4]. For any manifold located in a spherical region $r \in (r_s, 1.5r_s)$ the related braid group is trivial but for $r > 1.5r_s$ is equal to S_N , as usual in three dimensions. For $r > 1.5r_s$ the fermionic or bosonic quantum statistics can be assigned [5,9] contrary to the region $r \in (r_s, 1.5r_s)$.

The more detailed calculations from Appendix C are illustrated in Fig. 8; the upper curve (the red one in this figure) gives positions of stable circular orbits of a particle with small mass m , $m \ll M$ in the metric (15) (with respect to angular momentum of the particle \mathcal{L} , one of the motion integers), and the lower curve (the blue one) gives positions of unstable circular orbits (also with respect to \mathcal{L}). The upper curve (the red one) terminates in the point P at $r = 3r_s$. This point defines the innermost stable circular orbit. It is at $r = 3r_s$, $\mathcal{L} = \sqrt{3}mcr_s$, and energy (the second integer of a particle motion in gravitational field) $\mathcal{E}_0 = \sqrt{\frac{8}{9}}mc^2$ (point P in Fig. 8); cf. the derivation in Appendix C. The position of the innermost unstable circular orbit is at $r = 1.5r_s$ for $\mathcal{L} \rightarrow \infty$ and $\mathcal{E}_0 \rightarrow \infty$; it is an asymptotic value defined by the horizontal dotted line in Fig. 8, marked in green. The orbit $r = 1.5r_s$ is also the unstable circular orbit for photons (by taking the limit $m = 0$), thus it defines the photon sphere rim in the Schwarzschild metric.

The homotopy class of trajectories is immune to a change to distinct curvilinear coordinates at another choice of metric for the same gravitational singularity. The homotopy of trajectories is the same in arbitrary equivalent metric, precluding particle interchanges below the innermost unstable circular orbit. Hence, for the inner of the event horizon, where the dynamics of particles is also completely controlled by the central singularity and particles must unavoidably travel to the singularity point along short spirals towards the origin despite any value of energy and angular momentum of particular particles and any strength of interparticle interaction, the exchanges of particles are inaccessible. This is visible in Kruskal-Szekeres [43,44] or Novikov [42] coordinates. Interparticle interaction does not change the trajectory homotopy; though locally it can deform trajectories from its free particle shape, it cannot, however, produce closed cycles from one-way directed spirals governed in an overwhelming manner by central singularity both beneath the event horizon and beyond it up to the sphere with the radius of the innermost unstable circular orbit. This topological property, the qualitative change of the trajectory homotopy at the innermost unstable circular orbit, is schematically illustrated in Fig. 9.

Because of the division by the permutation group S_N in the definition of F_N space (3), this space is not intuitive, and differently numbered particle configurations are unified to the same point in F_N , which is counterintuitive. Despite such a limitation in the intuitive geometrization of braids, there must be available trajectories in M that are able to connect particle pairs at some fixed but arbitrary their numbering. In particular, they are needed to be possible for the exchange of two particles along two distinct oppositely directed trajectories in M joining these two particles when other particles are at rest. This pair of trajectories creates a local loop in M . Due to the indistinguishability of identical particles, if such a possibility exists for two selected particles, then it holds also for any other pair of particles. The existence of circular orbits (for $r \geq 1.5r_s$) ensures trajectory topology sufficient to particle interchange. Two particles located at the ends of an arbitrary diameter of a circle can exchange their positions along such semicircular trajectories (as illustrated in Fig. 9). The existence of circular trajectories (even if deformed by interparticle interaction) ensures in a topological sense the possibility of the nontrivial braid group implementation.

The closure of single-particle orbits in M does not mean the closure of loops in F_N , but some pieces of closed single-particle orbits in M (e.g., semicircles of circular geodesics) allow for the organization of elementary braids [of generators of the braid group σ_i , i.e., of exchanges of particles the i th with the $(i + 1)$ -th one at some fixed numbering of particles, conserving simultaneously positions of the rest of particles [5,9]]. In other words, the generators of the braid group, σ_i , $i = 1, \dots, N - 1$, are N -strand trajectory bunches exchanging only the i th particle with the $(i + 1)$ -th one when the other particles remain at rest, at arbitrary but fixed particle numbering. This exchange of the i th and $(i + 1)$ -th particles must be, however, available in the manifold M . It means that for a trajectory linking particle the i th with the $(i + 1)$ -th one in M , there must exist another trajectory linking inversely particle the $(i + 1)$ -th with the i th one; i.e., individual particle trajectories must be able to intersect at two points.

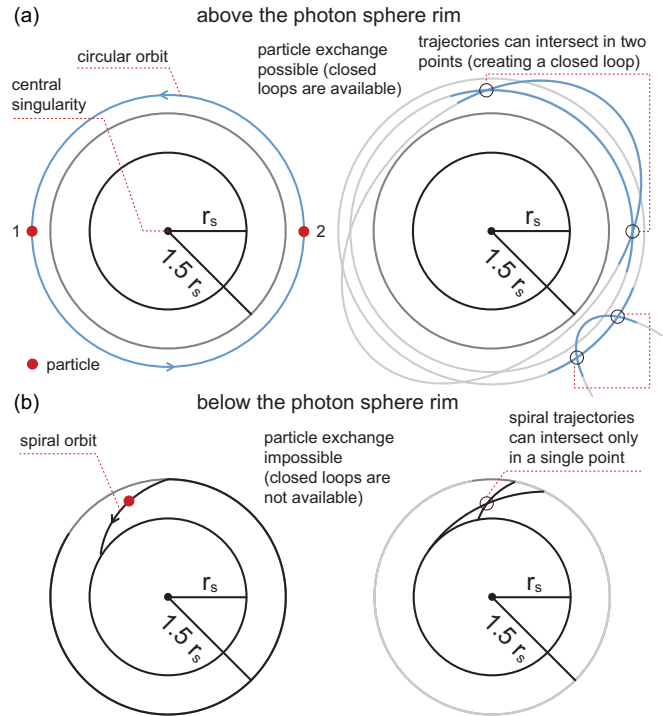


FIG. 9. Simplified pictorial illustration of the change of trajectory homotopy at passing the innermost unstable circular orbit of a black hole. If conic section-type trajectories are available, then the particle position interchanges are possible. Conic section-type trajectories beyond the photon sphere can intersect in two points, and local closed loops can be constructed from pieces of such trajectories (upper picture). When only short spiral trajectories are admitted beneath the photon sphere rim and particles unavoidably fall towards the event horizon (lower picture), then particles cannot mutually interchange positions (these spirals can intersect in only one point and do not create loops needed for particle exchange). Beyond the photon sphere circular orbits are possible, which topologically allows particle exchanges; beneath the innermost unstable circular orbit at $r = 1.5r_s$ (the rim of the photon sphere) none of the circular orbits are accessible.

Below the innermost unstable circular orbit (at $r = 1.5r_s$ for $\mathcal{L} \rightarrow \infty$) no closed orbit is possible. The dominating term in the effective potential [cf. Appendix C, Eqs. (C7) and (C8)] is here $\sim -\frac{\mathcal{L}^2}{r^3}$, which causes an unavoidable spiral movement towards the event horizon of any particle despite its energy and angular momentum and local mutual interaction between particles. The phase shift for such spirals is all the more limited the larger \mathcal{E}_0 for given \mathcal{L} . From pieces of these short spirals it is impossible to form any closed local loop required for local particle interchanges [spirals given by Eq. (C6) cannot intersect in two points simultaneously, in contrast to conic sections].

Outside the photon sphere closed loops are possible because trajectories are quasiconic sections which admit local closed loops formed from their pieces, which allows implementation of braids realizing particle interchanges. The photon sphere rim separates thus two distinct regions in the neighborhood of the black hole—the inner of the photon sphere simply connected and outer multiply connected. The

change of the homotopy class of the multiparticle configuration space causes local removal of the quantum statistics, which cannot be assigned for a trivial braid group [if $\pi_1(F_N) = \{\varepsilon\}$ then 1DUR must be $e^{i\alpha} = 1$, because $\varepsilon \cdot \varepsilon = \varepsilon$ for the neutral group element ε , which gives $2\alpha = \alpha$ and $\alpha = 0$; this is not bosonic statistics as ε does not describe any particle interchange]. In particular, no fermions or bosons can be assigned if particles cannot interchange.

VI. QUANTUM COLLECTIVE TRANSITION BENEATH THE INNERMOST UNSTABLE CIRCULAR ORBIT OF A BLACK HOLE

1DURs of the braid group determine quantum statistics of particles for which classical multiparticle trajectory loops in the configuration space F_N (exchanges of particles) are defined by this braid group [5,11,15]. For $\pi_1(F_N) = S_N$, as for arbitrary 3D M beyond the photon sphere, there exist two distinct scalar unitary representations, $\sigma_i \rightarrow e^{i0} = 1$ and $\sigma_i \rightarrow e^{i\pi} = -1$ defined on the generators of S_N , σ_i ($i = 1, \dots, N-1$), which are exchanges of the i th and $(i+1)$ -th particles. These two representations define bosons and fermions, respectively. The coincidence of these representations with the unitary irreducible representations of the rotation group $O(3)$ covered by $SU(2)$ in 3D space leads to the Pauli theorem on spin and statistics [45]. The linkage between representations of both groups is detailed in Appendix D. For $\pi_1(F_N) = \{\varepsilon\}$ as for M^* beneath the photon sphere rim of the black hole, the only existing representation is $\varepsilon \rightarrow 1$ (by virtue of $\varepsilon \cdot \varepsilon = \varepsilon$), and it does not define any quantum statistics, neither bosons nor fermions, because the trivial braid ε is not the exchange of particles.

Thus, for particles beneath the photon sphere rim [the sphere with the radius of the innermost unstable circular orbit in metric (15)] any quantum statistics of these particles cannot be assigned. This does not violate the Pauli theorem on spin and statistics, as the latter is not defined for a trivial braid group without any linkage to rotations in three dimensions governed over particle spin. In particular, fermions cannot be assigned, and particles with half spin lose their statistics.

The other theorem by Pauli, the so-called exclusion principle, asserts that quantum particles of fermionic type cannot share any common single-particle quantum state. Fermions cannot approach a space region already occupied by another fermion, and thus they mutually repulse themselves. This is called the quantum degeneracy repulsion, and the related pressure is the origin of stopping the collapse of white dwarfs or neutron stars. In the former case the degeneracy pressure of electrons plays the role [46], whereas in the latter case that of neutrons [47–49].

The exclusion principle for fermions leads also to the formation of the so-called Fermi sphere in the case of a large number of identical fermions in some volume, when the chemical potential μ (the energy increase by adding a single particle to the considered multiparticle system) is much greater than the temperature of the system in energy scale, $k_B T$, where k_B is the Boltzmann constant. In such a case, referred to as a quantum degenerate Fermi system, the particles are forced to occupy some consecutive in energy single-particle states one by one, resulting in the great accumulation

of the energy. For example, free electrons in a normal metal in room temperature with the typical concentration of order of 10^{23} (of order of the Avogadro number) per cm^3 constitute the large Fermi sphere with Fermi radius in momentum space $p_F \simeq 1.5 \times 10^{-24}$ kg m/s and with accumulated total energy $\sim 3 \times 10^{10}$ J/m³. This energy cannot be released in normal conditions because all fermions are blocked in their single-particle stationary states by the Pauli exclusion principle, i.e., all lower single-particle states are occupied, and thus there is no room for fermions to jump from higher energy states to lower ones.

The situation changes, however, when quantum statistics cannot be defined below the photon sphere rim of a black hole. When quantum statistics cannot be assigned in some space region, then in the system of indistinguishable fermions the Fermi sphere collapses entering this space region. The energy accumulated in the Fermi sphere can be released here.

The Fermi momentum p_F , the radius of the Fermi sphere in the degenerate homogeneous quantum liquid of fermions, depends only on particle concentration [16,50],

$$p_F = \hbar(3\pi^2\rho)^{1/3}, \quad (16)$$

where $\hbar = 1.05 \times 10^{-34}$ J s is the reduced Planck constant and $\rho = \frac{N}{V}$ is the concentration of fermions, i.e., N is the number of particles in the spatial volume V . The Fermi momentum is independent of the interaction of fermions according to the Luttinger theorem [50,51]. This follows from the fact that the phase space volume $V \frac{4}{3}\pi p_F^3$ with the position space volume V and the volume of momentum space of spherical shape $\frac{4}{3}\pi p_F^3$ corresponds to $n = \frac{V 8\pi p_F^3}{3h^3}$ of single-particle quantum states according to the Bohr-Sommerfeld rule [52] (here the additional factor 2 accounts for doubling of states for $\frac{1}{2}$ spin of fermions, and $h = 2\pi\hbar$ is the Planck constant). If all these states are filled, i.e., when $n = N$, then one gets (16). The formula for the Fermi momentum, as quasiclassically derived by the Bohr-Sommerfeld rule (immune to interaction), is independent of interaction of fermions in a Fermi liquid even with arbitrary strong particle interaction. With Fermi momentum the Fermi energy is linked, the kinetical energy of a particle with Fermi momentum (the chemical potential of fermions at $T = 0$ K is equal to the Fermi energy and weakly changes with the temperature growth [50]).

The whole Fermi sphere collects the energy per spatial volume V (neglecting interaction of fermions),

$$\begin{aligned} E &= \sum_{\mathbf{p}} \varepsilon(\mathbf{p}) f(\varepsilon(\mathbf{p})) \\ &= \frac{V}{(2\pi\hbar)^3} \int d^3\mathbf{p} \varepsilon(\mathbf{p}) f(\varepsilon(\mathbf{p})) \\ &= \int_0^{p_F} dp \int_0^\pi d\theta \int_0^{2\pi} d\phi p^2 \sin\theta \varepsilon(\mathbf{p}) \frac{V}{(2\pi\hbar)^3} \\ &= \frac{V}{2\pi^2\hbar^3} \int_0^{p_F} dp p^2 \varepsilon(p), \end{aligned} \quad (17)$$

where the sum runs over occupied states only, which is guaranteed by the Fermi-Dirac distribution function $f(\varepsilon(\mathbf{p})) = \frac{1}{e^{(\varepsilon(\mathbf{p})-\mu)/k_B T} + 1} \xrightarrow{T \rightarrow 0} 1 - \Theta[\varepsilon(\mathbf{p}) - \varepsilon_F]$ [here $\Theta(x)$ is the Heaviside step function and $\varepsilon_F = \varepsilon(p_F) = \mu(T = 0)$, and μ is the chemical potential], p, θ, ϕ are spherical variables in

TABLE I. Fermi momentum p_F [according to Eq. (16)], Fermi energy $\varepsilon_F = \varepsilon(p_F)$ [for the relativistic case of kinetic energy $\varepsilon(\mathbf{p}) = \sqrt{c^2 p^2 + m_n^2 c^4} - m_n c^2$, $m_n = 1.675 \times 10^{-27}$ kg, the mass of the neutron] and total energy of the Fermi sphere E [according to Eq. (17)] released at the decay of statistics for exemplary density ξ and radius r of a neutron star merger (n total number of neutrons in the star).

ξ [kg/m ³]	r [km]	n	p_F [kg m/s]	ε_F [GeV]	E [J]
5×10^{18}	10	1.13×10^{58}	4.52×10^{-19}	0.32	1.84×10^{47}
2×10^{18}	10	4.7×10^{57}	3.37×10^{-19}	0.2	4.8×10^{46}
1.0×10^{19}	8	1.08×10^{58}	5.57×10^{-19}	0.58	3×10^{47}
2.5×10^{18}	8	2.97×10^{57}	3.62×10^{-19}	0.24	3.5×10^{46}

momentum space, and $\varepsilon(\mathbf{p})$ is the kinetical energy of a fermion equal to $\frac{p^2}{2m}$ (in the nonrelativistic case), $\sqrt{p^2 c^2 + m^2 c^4} - mc^2$ (in the relativistic case) or cp (in the ultrarelativistic case). The factor $\frac{V}{(2\pi\hbar)^3}$ is the density of quantum states, i.e., the number of single-particle quantum states in the element of the phase space $V d^3\mathbf{p}$. The energy estimation (17) holds also for nonzero temperatures, if $k_B T \ll \mu \simeq \varepsilon_F$ (i.e., when a Fermi liquid is quantumly degenerated). For example, in metals $\varepsilon_F \simeq 90\,000$ K (in units assuming $k_B = 1$) and the Fermi sphere practically does not change even at the melting temperature.

In another example, a neutron star at the Tolman-Oppenheimer-Volkoff limit [47,48] with the density of order of 10^{18} kg/m³ (i.e., of the order of 2.3 Sun masses compressed to the compact neutron star with a radius of ca. 10 km), the neutron Fermi sphere energy attains the range of 10^{47} J, just as energy of frequently observed cosmic short giant gamma-ray bursts (assuming the isotropy of their sources); cf. Table I. The Fermi energy in this case $\varepsilon_F \simeq 3.7 \times 10^{12}$ K (at $k_B = 1$ units), which is much greater than the supposed temperature of the neutron star, of order of 10^6 K.

The same holds for any quantumly degenerated fermion system even at high temperature, i.e., when the chemical potential—the energy increase caused by addition a single particle to multiparticle statistical system [at $T = 0$ the chemical potential equals $\varepsilon_F = \varepsilon(p_F)$ and weakly depends on the temperature growth]—is much greater than the actual thermal energy $k_B T$, $k_B = 1.38 \times 10^{-23}$ J/K is the Boltzmann constant, and T is the absolute temperature in the system.

The coincidence of the energy stored in the Fermi sphere of neutrons in a neutron star at the Tolman-Oppenheimer-Volkoff limit with the energy of short giant gamma-ray bursts may support the concept that the source (yet unknown) of some of these bursts is a collapse of the Fermi sphere of neutrons when the total star is compressed to the volume inside its own photon sphere. At the decay of the Fermi sphere of neutrons, the latter liberated from the Pauli exclusion principle constraint fall apart on electrons and protons, charge particles interacting with the electromagnetic field. Rapidly allowed jumping of these particles onto their ground state at the decay of the neutron Fermi sphere will release a giant flux of isotropic electromagnetic radiation along the Fermi golden rule for quantum transitions [52], with the dominant component of gamma radiation because of the large value of Fermi energy in this case (cf. Table I).

The next example of the decay of a Fermi sphere of fermions at passing the photon sphere rim of a black hole

would be a quantum contribution to quasar luminosity. Quasars are sources of giant electromagnetic radiation, so they are visible from cosmological distances with luminosity exceeding hundreds of times the luminosity of a whole large galaxy. There are already known over a million quasars, the majority at a distance between 3 and 13 billion light years from us. Quasars are considered as supermassive active black holes (with mass of order of 10^9 Sun masses) consuming a surrounding matter, which fall down onto the gravitational singularity in the form of a vast accretion disk. Various channels of gravitational energy transfer to radiation from the accretion disk are taken into account, mostly due to temperature radiation of hot gas of electrons and ions heated to millions K due to matter compression. Nonthermal components of radiation are related with a bremsstrahlung or inverse Compton effect in the dense plasma close to the event horizon of the black hole, conventionally assumed at the distance not closer than $6r_s$.

If one considers an accretion disk of a quasar, then the density of electron and proton plasma (assuming accretion of neutral hydrogen) grows with falling of the matter towards the Schwarzschild horizon. The originally diluted neutral gas (of a hydrogen cloud) ionizes itself due to friction in the accretion disk and eventually becomes a degenerate Fermi liquid despite the high local temperature. This Fermi liquid attains an ultrahigh concentration in an increasingly flattened and compressed region in vicinity of the event horizon. For two-component plasma both Fermi spheres of electrons and protons contribute to the energy storage. At the same concentration of electrons and protons (due to the neutrality condition of plasma in the disk) electrons accumulate larger kinetic energy because of lighter mass [the relativistic kinetic energy of the electron and proton is $\varepsilon(\mathbf{p}) = \sqrt{c^2 p^2 + m^2 c^4} - mc^2$ with $m = m_e = 9.1 \times 10^{-31}$ kg and $m = m_p = 1.67 \times 10^{-27}$ kg, respectively]. The energy accumulated in the Fermi spheres of electrons and protons can be released in the form of the electromagnetic radiation if the Pauli exclusion principle is locally waived at the rim of the photon sphere, due to local decay of quantum statistics. Charged particles couple to a electromagnetic field, and the collapse of their Fermi spheres is accompanied with the emission of photons in agreement with the Fermi golden rule [52] for quantum transitions between initial states of particles in the Fermi sphere and their ground state.

In the case of quasars surrounded by the abundance of the matter as in the cosmological epoch, when accretion of the gas is limited only by the uppermost density of matter compression (similar to the density of neutron star at the

Tolman-Oppenheimer-Volkoff limit or to the density of atom nuclei), the continuous decay of Fermi spheres of electrons and protons in accretion plasma crossing the photon sphere of supermassive central black hole releases photons with total energy in the amount of 30% of infalling mass (quasars consume typically ca. 0.1 Earth mass per second, and 30% of this mass is converted into radiation). This radiation contributes to the luminosity of quasars with ca. 10^{40} W from the close vicinity of the event horizon (at the rim of the photon sphere at $r = 1.5r_s$ from the singularity) in better agreement with observations than only radiation from more distant regions of the accretion disk. The detailed quantitative estimation, including a general gravitation correction to the density at the innermost unstable circular orbit of the black hole, is presented in Appendix E.

The topological effect of the change of homotopy class of particle trajectories at passing the innermost unstable circular orbit of a black hole seems to modify also premises for the discussion of the information paradox for black holes and related problems. Since the illuminating papers of Hawking [53] and Bekenstein [54], who pointed out the entropy behavior of black holes in view of the second law of thermodynamics, the problem of the fate of information encoded in matter falling into a black hole is still open. The proposed temperature of black holes and the Hawking-Unruh radiation [53,55] are considered as breakthrough quantum properties of black holes. However, it has been proved [56] that this radiation is fully random, which causes the information paradox. Trials to solve it via the quantum entanglement of particle-antiparticle pairs at the event horizon and the escape of a particle associated by falling to the inside of the black hole of its antiparticle partner, encountered, however, problems with entanglement properties. Hawking radiation [53] has been resolved to the entanglement of two particles: escaping and falling into a black hole. Simultaneously, new Hawking radiation must be entangled with the old Hawking radiation, which leads to a conflict with the principle called “monogamy of entanglement.” To avoid this problem, the entanglement must somehow get immediately broken between the infalling particle and the outgoing particle. Breaking this entanglement would release large amounts of energy, thus creating a searing black hole firewall at the black hole event horizon [57]. This resolution causes, however, a violation of Einstein’s equivalence principle, which states that free falling is indistinguishable from floating in empty space. No entanglement between the emitted particle and previous Hawking radiation would require black hole information loss, a controversial violation of unitarity.

Polchinski with coauthors [57] stated that the paradox may eventually force us to give up one of three time-tested principles: Einstein’s equivalence principle, unitarity, or existing quantum field theory. The firewall concept is one possible information paradox solution. The Hawking-Unruh radiation has not been observed as of yet, and the firewall idea is still controversial as it breaks Einstein’s equivalence principle [57]. Moreover, the holographic formulation for quantum gravitation by Maldacena [58] strengthened the belief that the information should be conserved during the falling of matter into black holes in accordance with unitary quantum evolution. Thus, the fundamental premises of quantum mechanics

and of gravitation remain still in conflict in the case of black hole quantum behavior, which poses a significant problem for future quantum gravitation theory [57,58].

In the scenario proposed in the present paper, the matter deprived of quantum statistics at passing the photon sphere rim does not form a conventional system of particles but a specific quantum state of particles which cannot mutually interchange their positions, resembling an idealized perfect crystal in the third law of thermodynamics. For a remote observer the entropy of these particles would be even zero, if speculating they form a pure quantum state. Only due to the Unruh effect [55] the mixed state would be noticed by an accelerating observer (in particular, in a proper system attached to falling particles). The related Hawking-Unruh radiation is random [56], completely independent of a matter state but is related to the kinematic property in general relativity and the equivalence principle still holds at passing the event horizon. Instead at the rim of the photon sphere the radiation is released due to the decay of quantum statistics and waving out of the Pauli exclusion principle. This radiation is emitted according to the Fermi golden rule in an unitary manner. Thus, the entropy of the falling matter could be taken away with this radiation before crossing the event horizon. This radiation is somewhat similar to a firewall, but in distinction to that proposed by Polchinski and coauthors [57], it is visible for a remote observer (the Polchinski’s firewall must be invisible for a remote observer as it would associate the entanglement breaking at passing the event horizon, which is unobservable for a distant observer).

We do not go here to a conclusion as the problem of the entropy change at local disappearance of quantum statistics needs a separate consideration, but we can point only to some related aspects: (1) the information in condensed matter is encoded mainly in matter organized according to the Pauli exclusion principle, (2) the local waving out of quantum statistics restrictions allows the reducing of entangled states described by nonseparable symmetric and antisymmetric multiparticle wave functions of indistinguishable particles to separable states, and (3) at passing the photon sphere rim by a single particle in a pure state nothing happens, which does not violate the classical Einstein’s equivalence rule for such a particle.

VII. SUPPLEMENT TO THE CONVENTIONAL MODELS OF ACCRETION DISK AND COMPARISON WITH OBSERVATIONS

The collapse of Fermi spheres of degenerate Fermi systems at passing the innermost unstable circular orbit in the Schwarzschild metric (the photon sphere rim of a nonrotating uncharged black hole) does not conflict with the conventional models of the accretion disks of quasars [42,59]. The latter are based on the Shakura-Sunyaev classical hydrodynamic approach to plasma in an accretion disk [59], where the inverse transfer of the orbital momentum is modeled by friction and turbulence factors allowing the increase of plasma internal energy on the cost of the black hole gravitational energy [60–62]. Then hot plasma irradiates energy by thermal radiation [59,63]. This gives, however, only soft photons, and to elucidate giant luminosity of quasars (or microquasars) in

the x-ray range the mechanism of inverse Compton scattering of soft photons on hot electrons or ions is invoked [64]. The model of a hot accretion disk, originally proposed by Shapiro *et al.* for microquasar Cignus X-1 with a 15 Sun masses black hole [64], assumes an extremely high temperature of the inner part of the accretion disk (10^9 K for electrons and 10^{11} K for ions) to ensure sufficient energy of charge carriers needed for Comptonization of soft photons (the identification of a sufficiently abundant soft photon source is not clear, however). Though the Comptonization mechanism in this hot accretion disk model is adjusted to x-ray radiation luminosity of Cignus X-1, the generalization of the model to extremely luminous giant quasars with supermassive black holes ($\sim 10^9$ Sun masses or larger) [65] is problematic, since the temperature 10^9 – 10^{11} K of hot plasma in a vast disk seems to be unrealistic. Nevertheless, some numerical simulations of developments of the Shakura-Sunyaev and Thorne-Novikov model [42,59] done recently by Fragile *et al.* [66], allow one to match observable luminosities of some not distant ($z < 0.3$) active binary black hole objects [67], but rather not superluminous remote quasars [65]. Higher radiation efficiency has been modeled within a conventional classical magneto-hydrodynamic approach by inclusion of a hypothetical giant magnetic component to accretion plasma in the case of a spinning black hole [68], assuming, however, an unrealistic accretion mass rate to gain sufficiently large luminosity.

All hydrodynamic or magneto-hydrodynamic models of matter accretion onto a black hole are applicable, however, only relatively far from the event horizon of the black hole. In all such models the inner edge of the accretion disk is assumed to be located well above the photon sphere of the black hole (the latter coincides with the radius of the innermost unstable circular orbit in the Schwarzschild metric, at $r = 1.5r_s$, $r_s = \frac{2GM}{c^2}$), i.e., even more distant than the innermost stable circular orbit with the radius $3r_s$ (conventionally assumed the inner edge of the accretion disk is at $\sim 6r_s$ [64]).

The collapse of the Fermi spheres described in the present paper takes place at the rim of the photon sphere at $r = 1.5r_s$, in the region completely neglected in conventional hydrodynamic models of matter accretion [42,59,66,68], thus this mechanism does not interfere with thermal (including bremsstrahlung) and Comptonization mechanisms for radiation emission from more distant parts of the accretion disk (typically for $r > 6r_s$). Inclusion of the quantum effect of Fermi sphere collapse at the photon sphere rim ($r = 1.5r_s$) can, however, considerably supplement developments of the Shakura-Sunyaev-Thorne-Novikov classical hydrodynamic approach [42,59] not applicable in proximity of the event horizon. The release of high-energy photons (depending on the accretion mass rate, the black hole mass, and governed by the Fermi momentum in compressed plasma) due to Fermi sphere collapse can add to the total luminosity of quasars and microquasars, allowing for the avoidance of some parameter-fitting problems and shortages of conventional classical models [66,68].

The rejection of the quantum statistics in a system of indistinguishable identical particles at passing the rim of the photon sphere is a general property of any black hole, regardless of its mass. The energy per unit volume stored in the Fermi sphere of a degenerate Fermi system is a monotonic function of the

density of matter. Its maximum is attained for the uppermost possible density of compressed electron-hadron plasma, as in extremely bright quasars or in the case of neutron star mergers exceeding the Tolman-Oppenheimer-Volkoff stability limit (the uppermost density of compressed Fermi liquid is of the order of the density of hadrons in atom nuclei). In the case of quasars the collapse of electron and proton Fermi spheres in the stream of ionized matter in an accretion disk gives the steady luminosity $\sim 10^{40}$ W for $\sim 10^9$ Sun masses supermassive black holes consuming ca. 10 Sun masses per year (0.1 Earth mass per second) for a long time (as assessed in Appendix E). In the case of a neutron star merger which exceeds the Tolman-Oppenheimer-Volkoff limit of ca. 2.3 Sun masses compressed to uppermost density of hadrons, the merger rapidly collapses due to the relief of internal pressure caused by local recall of the Pauli exclusion principle, when the entire star is smaller than its own photon sphere. The released energy due to collapse of a neutron Fermi sphere in the neutron star merger reaches 10^{47} J; cf. Table I (this energy partly escapes from the photon sphere of a rising black hole in the form of a short giant burst of gamma rays). In both these extremal cases of the matter compression (in superluminous quasars and at collapse of neutron star mergers) the efficiency of mass to radiation conversion is ca. 30%, not achievable in any other physical mechanism except for matter-antimatter annihilation (the efficiency of nuclear fusion in stars is only of order of 0.7% for the mass to energy conversion rate).

In the case of not extremal matter compression in the accretion disk of black holes (as in many active galactic nuclei or in microquasars with a lower rate of the matter influx) the radiation emitted due to Fermi sphere collapse is less intensive (the mass to energy conversion rate is lower than 30%) and softer, but still contributes to the total luminosity and can help to explain radiation properties of observed binary black hole systems [65,67]. In particular, the Fermi sphere collapse can help to elucidate the relatively short-lasting brightening of active galactic nuclei, like the recently observed for AGN IES 1927+654 [69]. The 100-fold increase of its luminosity within a few months period would be associated with accidental increase of the matter consumption rate during the corresponding time. If this accidental matter influx is not extremal, then photons emitted due to the Fermi sphere collapse may not reach over-MeV energy and are not able to produce electron-positron pairs in the ergosphere of this spinning black hole. However, the massive isotropic flux of lower energy photons caused by the Fermi sphere collapse of electrons and protons may push electron-positron pairs created in the ergosphere according to the Blandford-Znajek electromagnetic mechanism [70] towards the event horizon, lowering in this way their evaporation to jets across ergosphere nodes. The model by Blandford-Znajek [70] gives the theory of jet formation for spinning Kerr-like black holes, where due to dragging of the reference frame in a Kerr metric the magnetic field carried with the accretion matter rotates. The rotation of the ergosphere causes the magnetosphere inside it to rotate, and the outgoing flux of angular momentum results in extraction of energy from the black hole. The magnetic field beams in the form of jets and electrons and positrons diffuse across nodes of the ergosphere and next are highly accelerated in magnetic field beams in jets producing intensive x-ray

radiation. The hypothetical source of electron-positron pairs is a strong electrical field created by the rotating magnetic field frozen in the ergosphere. The sufficient intensity of the electric field to generate particle-antiparticle pairs in the ergosphere is, however, speculative. A collapse of Fermi spheres in plasma approaching the Kerr black hole would be helpful here, as it can supply the abundance of over-MeV photons in the case of extreme matter influx, when the energy of these released photons can reach GeV level and can produce a large number of electron-positron pairs, which are able to power up jets besides the Blandford-Znajek mechanism. Nevertheless, in the case when the released photons are sub-MeV at a smaller rate of matter consumption by a black hole, then they cannot produce additional electron-positron pairs inside the ergosphere but can push towards the event horizon those created according to the Blandford-Znajek mechanism, reducing their supply to jets. This could explain the temporal change in the radiation spectrum during a brightening episode consisting in an optical 100-fold increase of the optical luminosity and simultaneous lowering of x-ray radiation (the latter probably due to reduction of the amount of electrons and positrons in the jet, the source of x-ray radiation in jets), without the need to speculate on remagnetization of the AGN and quenching of its jets by an oppositely magnetized gas cloud during this episode [69]. When the Fermi energy in accreting plasma does not exceed MeV, then the collapse of a Fermi sphere can produce an increase of the luminosity with lower frequency (just as has been observed for AGN IES 1927 + 654) and, simultaneously, can temporarily reduce the intensity of x-ray radiation from jets, also in agreement with observations.

VIII. CONCLUSIONS

The important role of the availability of classical trajectories for Feynman path integrals is demonstrated. This method of quantization is especially convenient to identify quantum effects rooted in topological homotopy-type constraints imposed onto trajectories which enter functional integrals. Despite some popular belief, not all trajectories can contribute to path integrals, but only those which are classically accessible. This is visible in the path integral approach to single-particle tunneling across barriers and in path integral generalization to multiparticle systems. For indistinguishable identical particle systems, path integrals are especially sensitive to constraints imposed on trajectories by their topological homotopy properties. The paths in this case are linked to so-called braids displaying indistinguishability of particles leading to quantum statistics and correlation phenomena. In topologically rich systems of interacting 2D electrons exposed to a strong magnetic field, the availability of braids is changing with varying magnetic field value. Braid trajectories are admitted only at the commensurability of multiloop cyclotron orbits with distribution of interacting electrons in two dimensions, which results in the definition of complete FQHE hierarchy. The consistency of such topological approach with experimental observations of FQHE in conventional semiconductor 2D systems, in a graphene monolayer and bilayer, and even in fractional Chern topological insulators (in which the magnetic field is substituted by the Berry field) evidences a topological character of quantum Hall physics.

Another consequence of the homotopy restrictions imposed on classical trajectories occurs in spacetime folded by general-relativity gravitational singularity. The homotopy transition between a multiply and simply connected configuration space of identical indistinguishable particle systems at passing the photon sphere rim of a black hole results in high-energy phenomena, which can help clarify the astrophysical observations. This homotopy transition results in a quantum mechanism of transfer of gravitation energy into radiation in the accretion disk of a black hole with the efficiency up to 30% mass to energy conversion rate, which is actually encountered in superluminous quasars and is beyond the explanation ability of conventional models of quasar luminosity. The same mechanism can be responsible for the creation of some kind of giant gamma-ray bursts (their source is unknown as of yet) at neutron star merger collapses, when also ca. 30% of the merger mass is converted into radiation. The agreement with these two independent astrophysical high-energy phenomena supports the model of Fermi sphere decay in the vicinity of a black hole due to the change of the availability of braid trajectories for indistinguishable particles approaching the event horizon.

The spin and statistics are closely related as pointed out in Pauli theorem. This theorem holds not only in three dimensions where exclusively fermion- and boson-type statistics are available, but also in two dimensions where fractional anyon statistics are admitted, in agreement, on the other hand, with nonquantized spin in two dimensions [related with $U(1)$ rotational symmetry]. In the 2D case of charged indistinguishable particles exposed to a magnetic field (or Berry field in topological Chern insulators) the Pauli theorem must be again generalized to account for specific quantum statistics responsible for fractional quantum Hall effect (including composite fermions and their generalizations) and fractional Chern insulators. Spin of particles is governed by a rotational group independently of constraints imposed on braid properties of particles as is illustrated in the case of a general relativistic gravitation singularity. Similarly for a single particle the spin can be well defined but not the quantum statistics. From these examples it follows that quantum statistics of the same classical particles can change in response to the topological constraints imposed on the multiparticle system. This reflects the fundamental role of the availability or restrictions regarding the identical particle exchanges and expressed in homotopy braid group terms, which for a multiparticle system of indistinguishable particles can vary in response to topological constraints and can modify quantum statistics of the same classical counterparts.

APPENDIX A: SIZE OF CYCLOTRON ORBITS FOR 2D ELECTRONS

Let us consider a 2D electron in a perpendicular magnetic field B . The x and y components of its kinematic momentum are [for vector potential in Landau gauge $\mathbf{A} = (0, -Bx, 0)$, $\mathbf{B} = \text{rot } \mathbf{A} = (0, 0, B)$]

$$\begin{aligned} P_x &= -i\hbar \frac{\partial}{\partial x}, \\ P_y &= -i\hbar \frac{\partial}{\partial y} - eBx. \end{aligned} \quad (\text{A1})$$

The commutator $[P_x, P_y]_- = i\hbar eB$ (it is invariant with respect to magnetic field gauge). Two variables $Y = \frac{P_x}{eB}$ and P_y are conjugated, as $[Y, P_y]_- = i\hbar$, and they can be considered as generalized 1D position and momentum. By application of the Bohr-Sommerfeld rule [52] to this generalized 1D phase space, one obtains

$$\Delta S_{Y, P_y} = \Delta \oint P_y dY = h, \quad (\text{A2})$$

where $\Delta S_{Y, P_y}$ is the smallest portion of the 1D phase space (Y, P_y) , $h = 2\pi\hbar$. The phase space (Y, P_y) is in fact the renormalized space (P_x, P_y) . The closed trajectory in (P_x, P_y) space is repeated in the space (x, y) , with the renormalization factor $\frac{1}{(eB)^2}$ and turned by the angle $\pi/2$, because of the Lorentz force, $\mathbf{F} = \frac{d\mathbf{P}}{dt} = e \frac{d\mathbf{r}}{dt} \times \mathbf{B}$, where $\mathbf{r} = (x, y)$ and $\mathbf{P} = (P_x, P_y)$.

Thus, from (A2) one obtains

$$\Delta S_{x, y} = \Delta \oint y dx = \frac{h}{eB}, \quad (\text{A3})$$

which is the smallest 2D cyclotron orbit in (x, y) of an electron ($\Delta S_{x, y} B = \Phi_0 = \frac{h}{e}$ is the magnetic field flux quantum).

The cyclotron orbit (A3) is single-loop. If, however, the elementary trajectory between turning points in the Bohr-Sommerfeld rule is the path with additional k loops, then the smallest piece of 1D phase space (Y, P_y) is $(2k+1)h$ [32]. Such a situation happens when loopless σ_i braids cannot match the nearest neighbors in Wigner lattice. The elementary trajectory in this case can be σ_i^{2k+1} , i.e., the cyclotron braid with additional k loops, and such a simplest trajectory must be taken in the Bohr-Sommerfeld rule instead of σ_i , which results in $(2k+1)$ times larger size of the phase space orbit. Hence, instead of (A3) one obtains

$$\Delta S_{x, y} = \frac{(2k+1)h}{eB}, \quad (\text{A4})$$

which defines the size of $(2k+1)$ -loop cyclotron orbit $(\sigma_i^{2k+1})^2$ (the effective magnetic field flux quantum in the correlated state of electrons defined by braid generators σ_i^{2k+1} equals $\Phi_k = \frac{(2k+1)h}{e}$).

The sizes of cyclotron orbits, single-loop (A3) and $(2k+1)$ -loop (A4), refer to the LLL. In higher LLs cyclotron orbits are proportional to the factor $(2n+1)$, with n , the Landau index, because the kinetic energy in consecutive LLs scales linearly with Landau index, just $\sim(2n+1)$. Hence the cyclotron orbit size in arbitrary LLs equals

$$\Delta S_{x, y} = (2n+1)(2k+1) \frac{h}{eB}, \quad (\text{A5})$$

where n is the Landau index, $(2k+1)$, the number of loops in the orbit.

Note that the size of cyclotron orbit in particular LLs is immune to interparticle interaction in a collective state of electrons, because the Bohr-Sommerfeld rule holds independently of interaction (as the quasiclassical approximation is not perturbative with respect to interaction). In 2D systems of interacting electrons, cyclotron orbits can be deformed but their surface (A5) is conserved and universal.

APPENDIX B: GENERAL FORM OF CYCLOTRON BRAID GENERATORS FOR ADMISSIBLE TRAJECTORIES FOR 2D INTERACTING ELECTRONS IN MAGNETIC FIELD AND CORRESPONDING WAVE FUNCTIONS FOR FQHE HIERARCHY IN THE LLL

The general homotopy invariant for cyclotron electron correlations of 2D electrons has the form as given by Eq. (13),

$$\frac{BS}{N} = \frac{h}{x_1 e} \pm \frac{h}{x_2 e} \pm \dots \pm \frac{h}{x_q e}, \quad (\text{B1})$$

where $q = 2k+1$ is the number of loops of cyclotron orbit and x_i indicates the fraction of next-nearest neighbors in a Wigner lattice commensurate with the i th loop. The form of the invariant (B1) results from the commensurability condition for a single-loop cyclotron orbit with next-nearest neighbors of some rank. If the total number of these neighbors is $\frac{N}{x}$, then the single-loop commensurability condition is $\frac{BS}{N/x} = \frac{h}{e}$, which gives the form of components (each per single loop) in (B1). The \pm in (B1) indicates a possible inverted ($-$) or congruent ($+$) circulation of a loop with respect to the preceding one.

To the invariant (B1) corresponds the filling rate given by Eq. (14),

$$\nu = \left(\frac{1}{x_1} \pm \frac{1}{x_2} \pm \dots \pm \frac{1}{x_q} \right)^{-1}, \quad (\text{B2})$$

because $\nu = \frac{N}{N_0}$ and the degeneracy of LLs, $N_0 = \frac{BS_e}{h}$.

To the invariant (B1) there correspond generators for the related cyclotron subgroup, which have the following form:

$$\begin{aligned} b_j &= (\sigma_j \sigma_{j+1} \dots \sigma_{j+x_i-2} \sigma_{j+x_i-1} \sigma_{j+x_i-2}^{-1} \dots \sigma_j^{-1}) \\ &\quad \times (\sigma_j \sigma_{j+1} \dots \sigma_{j+x_i-2} \sigma_{j+x_i-1} \sigma_{j+x_i-2}^{-1} \dots \sigma_j^{-1})^{\pm 1} \\ &\quad \dots \\ &\quad \times (\sigma_j \sigma_{j+1} \dots \sigma_{j+x_q-2} \sigma_{j+x_q-1} \sigma_{j+x_q-2}^{-1} \dots \sigma_j^{-1})^{\pm 1}, \\ j &= 1, \dots, N' \quad N' = N - \max(x_i), \end{aligned} \quad (\text{B3})$$

where the segment

$$(\sigma_j \sigma_{j+1} \dots \sigma_{j+x_i-2} \sigma_{j+x_i-1} \sigma_{j+x_i-2}^{-1} \dots \sigma_j^{-1}) \quad (\text{B4})$$

defines the exchange of the j th electron with the $(j+x_i)$ -th one as prescribed in (B1) for the i th loop of a q -loop cyclotron orbit. For $x_i = 1$ (the nearest neighbors) this segment (B4) is simply σ_j .

The generators (B3) define elementary exchanges of electrons. Not all transpositions are possible but only those defined by the generators. Scalar unitary representation of generators (B3) is $e^{i(1 \pm 1 \pm \dots \pm 1)\pi}$, as for original electrons $\sigma_j \rightarrow e^{i\pi}$ and $\sigma_j^{-1} \rightarrow e^{-i\pi}$. Therefore, the segment (B4) must generate the polynomial factor to the multiparticle wave function,

$$\prod_{j=1, k=1; j < \text{mod}(j, x_i, 1) + (k-1)x_i}^{N', N/x_i} (z_j - z_{\text{mod}(j, x_i, 1) + (k-1)x_i}) \quad (\text{B5})$$

[N' is the collection of admissible values of j at which the generator (B3) can be defined; it is equal to $N - \max(x_i)$ for

x_i entering (B3)] as the projective scalar unitary representation of this segment is $e^{i\pi}$ (or $e^{-i\pi}$ if it enters as an inverted operator). In the above formula $\text{mod}(j, x_i, 1)$ is the rest of the division of j by x_i with offset 1. Thus the total multiparticle wave function corresponding to generators (B3) acquires the form

$$\begin{aligned} & \Psi(z_1, \dots, z_N) \\ &= \mathcal{A} \prod_{j=1, k=1; j < \text{mod}(j, x_1, 1) + (k-1)x_1}^{N', N/x_1} (z_j - z_{\text{mod}(j, x_1, 1) + (k-1)x_1}) \\ & \times \prod_{j=1, k=1; j < \text{mod}(j, x_2, 1) + (k-1)x_2}^{N', N/x_2} (z_j - z_{\text{mod}(j, x_2, 1) + (k-1)x_2}) \\ & \times \dots \\ & \times \prod_{j=1, k=1; j < \text{mod}(j, x_q, 1) + (k-1)x_q}^{N', N/x_q} (z_j - z_{\text{mod}(j, x_q, 1) + (k-1)x_q}) \\ & \times e^{-i \sum_{i=1}^N |z_i|^2 / 4l_B^2}, \end{aligned} \quad (\text{B6})$$

for both two possibilities of scalar unitary representations related to \pm in (B1) causing only an unimportant change of sign.

One can notice from Eq. (B6) that in the case of $x_1 = x_2 = \dots = x_q = 1$ and only $+$ instead of \pm in (B1), the Laughlin function is reproduced for $\nu = \frac{1}{q}$. The envelope part of function (B6), $e^{-i \sum_{i=1}^N |z_i|^2 / 4l_B^2}$, is correct only in GaAs, and this envelope changes in graphene according to the different explicit form of single-electron LL functions in graphene [71].

The examples of the wave function (B6) for various ν from the general FQHE hierarchy given by Eq. (B2) are presented in Ref. [33] including the related energy calculation.

APPENDIX C: HOMOTOPY OF PARTICLE

TRAJECTORIES IN THE VICINITY OF THE EVENT HORIZON IN SCHWARZSCHILD METRIC: DERIVATION

Let us consider trajectories of particles (with mass m vanishingly small in comparison to central mass M) in the upper neighborhood of the Schwarzschild event horizon. These trajectories coincide with geodesics in the metric (15). Because of the spherical symmetry of the gravitational field described by (15) these geodesics must lie in planes and without any loss of generality one can consider the geodesic plane $\theta = \frac{\pi}{2}$. The geodesics for a particle with the mass m can be determined in various equivalent classical dynamics formulations, e.g., by solution of the Hamilton-Jacobi equation,

$$g^{ik} \frac{\partial S}{\partial x^i} \frac{\partial S}{\partial x^k} - m^2 c^2 = 0, \quad (\text{C1})$$

with g^{ik} metric tensor components corresponding to metric (15) [72]. Equation (C1) attains for the Schwarzschild metric (15) the following form:

$$\begin{aligned} & \left(1 - \frac{r_s}{r}\right)^{-1} \left(\frac{\partial S}{\partial t}\right)^2 - \left(1 - \frac{r_s}{r}\right) \left(\frac{\partial S}{\partial r}\right)^2 - \frac{1}{r^2} \left(\frac{\partial S}{\partial \phi}\right)^2 \\ & - m^2 c^2 = 0, \end{aligned} \quad (\text{C2})$$

with the function S in the form

$$S = -\mathcal{E}_0 t + \mathcal{L} \phi + S_r(r). \quad (\text{C3})$$

In the above formula the quantities \mathcal{E}_0 and \mathcal{L} are the particle energy and its angular momentum, respectively. \mathcal{E}_0 and \mathcal{L} are constants of motion. Equation (C1) can be also applied to define trajectories of photons assuming in (C1) $m = 0$.

If one substitutes Eq. (C3) into Eq. (C2), then one can find $\frac{\partial S_r}{\partial r}$. By the integration of this formula one obtains

$$S_r = \int dr \left[\frac{\mathcal{E}_0^2}{c^2} \left(1 - \frac{r_s}{r}\right)^{-2} - \left(m^2 c^2 + \frac{\mathcal{L}^2}{r^2}\right) \left(1 - \frac{r_s}{r}\right)^{-1} \right]^{1/2}. \quad (\text{C4})$$

Geodesics are thus defined by the condition $\frac{\partial S}{\partial \mathcal{E}_0} = \text{const}$, which gives radial dependence of the trajectory $r = r(t)$, and by the condition $\frac{\partial S}{\partial \mathcal{L}} = \text{const}$, determining the angular dependence $\phi = \phi(t)$ of the particle trajectory. The condition $\frac{\partial S}{\partial \mathcal{E}_0} = \text{const}$ gives

$$ct = \frac{\mathcal{E}_0}{mc^2} \int \frac{dr}{\left(1 - \frac{r_s}{r}\right) \sqrt{\left(\frac{\mathcal{E}_0}{mc^2}\right)^2 - \left(1 + \frac{\mathcal{L}^2}{m^2 c^2 r^2}\right) \left(1 - \frac{r_s}{r}\right)}}. \quad (\text{C5})$$

The condition $\frac{\partial S}{\partial \mathcal{L}} = \text{const}$ results in the relation

$$\phi = \int dr \frac{\mathcal{L}}{r^2} \left[\frac{\mathcal{E}_0^2}{c^2} - \left(m^2 c^2 + \frac{\mathcal{L}^2}{r^2}\right) \left(1 - \frac{r_s}{r}\right) \right]^{-1/2}. \quad (\text{C6})$$

Equation (C5) can be rewritten in a differential form,

$$\frac{1}{1 - r_s/r} \frac{dr}{cdt} = \frac{1}{\mathcal{E}_0} \left[\mathcal{E}_0^2 - U^2(r) \right]^{1/2}, \quad (\text{C7})$$

with the effective potential,

$$U(r) = mc^2 \left[\left(1 - \frac{r_s}{r}\right) \left(1 + \frac{\mathcal{L}^2}{m^2 c^2 r^2}\right) \right]^{1/2}, \quad (\text{C8})$$

where \mathcal{E}_0 and \mathcal{L} are energy and angular momentum of the particle, respectively.

Equation (C7) allows for the definition of an accessible region for the motion via the following condition, $\mathcal{E}_0 \geq U(r)$. Moreover, the condition $\mathcal{E}_0 = U(r)$ defines circular orbits. Limiting circular orbits can be thus found by the determination of extrema of $U(r)$. Maxima of $U(r)$ define unstable orbits, whereas minima stable ones (depending on parameters \mathcal{E}_0 and \mathcal{L} , which are integrals of the motion). The conditions $U(r) = \mathcal{E}_0$ and $\frac{\partial U(r)}{\partial r} = 0$ (for extreme) attain the explicit form

$$\begin{aligned} & \mathcal{E}_0 = \mathcal{L} c \sqrt{\frac{2}{r r_s}} \left(1 - \frac{r_s}{r}\right), \\ & \frac{r}{r_s} = \frac{\mathcal{L}^2}{m^2 c^2 r_s^2} \left[1 \pm \sqrt{1 - \frac{3m^2 c^2 r_s^2}{\mathcal{L}^2}} \right], \end{aligned} \quad (\text{C9})$$

where the sign $+$ in the second equation corresponds to stable orbits [minima of $U(r)$] and the sign $-$ to unstable ones [maxima of $U(r)$]. Positions of stable and unstable circular orbits depend on energy \mathcal{E}_0 and angular momentum \mathcal{L} .

This is illustrated in Fig. 8; the upper curve (red one in this figure) gives positions of stable circular orbits (with respect to

angular momentum \mathcal{L}) and the lower curve (blue one) gives positions of unstable circular orbits (also with respect to \mathcal{L}). The related value of \mathcal{E}_0 is given by the first equation of the system (C9).

APPENDIX D: PAULI THEOREM ON CONNECTION BETWEEN STATISTICS AND SPIN

Pauli theorem on spin-statistics connection [45] states that quantum statistics of particles with half spin must be of fermionic type, while those of particles with integer spin of bosonic type. This theorem is supported by the quantum relativistic reasoning that within the Dirac electrodynamics for spinor-described particles, the Hamiltonian formulation is admitted for simultaneously particles and antiparticles, and to ensure positively defined kinetic energy of free particles, the field operators defining particles (and antiparticles) must anticommute, and thus are of fermionic type [73]. Such a proof is confined, however, to free particles and to 3D position space, the manifold on which particles are located. A wide discussion of Pauli theorem on spin-statistics connection including various trials of its proof is presented in [74,75], where also a rigorous proof of this theorem in the case of noninteracting particles is provided. The Pauli theorem holds, however, also for arbitrarily strongly interacting particles. This is visible in terms of topology as the actual proof of Pauli theorem must invoke homotopy-type reasoning in view of a braid group-based quantum statistics definition [76]. The Pauli theorem follows from the coincidence of unitary irreducible representations of the rotation group, which define quantization of spin or angular momentum [77] with unitary representations of braid groups nominating quantum statistics [5]. The agreement between unitary representations of both groups arises due to the overlap of some elements of the braid group and the rotation group. The representations which are uniform on group generators must thus agree for whole groups. The half spin representation of the rotation group must agree with the odd representation $e^{i\pi} = -1$ of the braid group for 3D manifold (and fermions), whereas the integer angular momentum representation of the rotation group must agree with even $e^{i0} = 1$ representation of the permutation group (and bosons). Such an approach allows simultaneously for the extension of Pauli theorem onto 2D manifolds with anyons (which, in general, are neither fermions nor bosons). For 2D position space the rotation group is Abelian, which causes that spin in two dimensions is not quantized and perfectly agrees with the continuous scalar unitary representations of the Artin braid group defining anyon fractional statistics. Such a topological proof of Pauli theorem is immune to particle interaction.

To be more specific, let us note that for 3D manifolds, the rotation group $O(3)$ has the covering group $SU(2)$, and the irreducible unitary representations of $SU(2)$ fall into two classes assigning integer and half-integer angular momenta. These two classes agree with only two possible scalar unitary representations of the permutation group S_N , which is the braid group for 3D manifolds. The representations of both groups coincide as they have some common elements. However, for 2D manifolds the rotation group $O(2)$ is Abelian and isomorphic with the $U(1)$ group possessing just the same

continuous unitary representations $e^{i\alpha}$, $\alpha \in [0, 2\pi)$, as the Artin group, which is the braid group for $M = R^2$. Thus, in 2D space the Pauli theorem also holds for not quantized spin assigned by $s = \frac{\alpha}{2\pi}$ and similarly continuously changing anyon statistics defined by $e^{i\alpha}$ numbered by $\alpha \in [0, 2\pi)$.

Quantum statistics and spin, though they coincide via the agreement between unitary representations of rotation and braid groups, are in fact independent to some extent, and one can imagine a situation when the spin is still defined but the statistics is not, as in the case of the absence of a nontrivial braid group. Such a situation occurs in an extremely strong gravitational field inside the black hole and close to its event horizon, beneath the photon sphere rim, as is demonstrated in the present paper.

APPENDIX E: ASSESSMENT OF EFFICIENCY OF THE COLLAPSE OF FERMI SPHERES OF ELECTRONS AND PROTONS IN THE ACCRETION DISK CLOSE TO EVENT HORIZON OF A QUASAR INCLUDING GENERAL-RELATIVISTIC CORRECTIONS

The matter falling onto the black holes of superluminous quasars must convert up to ca. 30% of its mass into radiation to explain its observable luminosity and simultaneously the rate of the increase of central black hole mass over a long time period of their activity to be consistent with observed masses of supermassive black holes in galaxies. As the giant black holes in nearer galaxies are of a size at most on the order of billions masses of the Sun, the estimation of the mass consumption rate for quasars with luminosity of order of 10^{40} W is typically ca. 10 Sun masses per year (i.e., of order of 0.1 Earth mass per second), in an extreme case of 1000 Sun masses per year (10 Earth masses per second).

Central black holes in quasars vary between 10^5 – 10^9 of solar masses, as have been measured using a reverberation mapping. Several dozen nearby large galaxies, including our own Milky Way, that do not have an active center and do not show any activity similar to a quasar, are confirmed to contain similar supermassive black holes in their centers. Thus it is now thought that all large galaxies have giant black holes of this kind, but only a small fraction have sufficient matter in the right kind of orbit at their center to become active and power radiation in such a way as to be seen as quasars.

For concreteness of the estimation let us assume that the central black hole in a quasar consumes $5.6 M_\odot$ per year, i.e., ca. 0.06 Earth mass per second. Let us assume the stable uniform in time process of matter accretion. The transport of matter across the disk is steady, thus we can perform calculations, e.g., per a single second. Using Eqs. (16) and (17) one can assess the energy stored in the Fermi spheres for electrons and protons, if all the electrons and protons from the gas mass equal 0.06 Earth mass, are compressed to the spatial volume V per second. The local Fermi momentum

$$p_F(r) = \hbar(3\pi^2\rho(r))^{1/3} = \hbar\left(3\pi^2\frac{n}{V(r)}\right)^{1/3}, \quad (E1)$$

where r is the distance from the center. $p_F(r)$ is constant in time and grows across the disk with increasing local concentration $\rho(r) = \frac{dn}{dV} = \frac{n}{V(r)}$, the same for electrons and protons.

The latter equality holds for steady accretion, and n is the total number of electrons (or protons) per second, compressed in total to the volume $V(r)$ at the distance r from the origin with central gravitational singularity. This means that portions dn of electrons and protons in infinitely small consecutive periods dt incoming in radial direction towards the central singularity compressed to dV at radius r add up in a single second time period to the total constant flow of mass (in the example, of $0.06 \times M_Z$ kg/s, the Earth mass $M_Z = 5.97 \times 10^{24}$ kg), and as the whole is compressed locally at r to the volume $V(r)$. The locally accumulated energy in the Fermi spheres of electrons and protons grows with lowering r due to the increase of the compression caused by the gravitational field. This energy is proportional to $V(r)$ and, moreover, depends on $V(r)$ via the local Fermi momentum (E1) and in accordance with Eq. (17) can be written as

$$\begin{aligned} E(r) &= E_e(r) + E_p(r), \\ E_e(r) &= \frac{V(r)}{2\pi^2\hbar^3} \int_0^{p_F(r)} dp p^2 \left(\sqrt{p^2 c^2 + m_e^2 c^4} - m_e c^2 \right), \\ E_p(r) &= \frac{V(r)}{2\pi^2\hbar^3} \int_0^{p_F(r)} dp p^2 \left(\sqrt{p^2 c^2 + m_p^2 c^4} - m_p c^2 \right), \end{aligned} \quad (\text{E2})$$

where the energy $E_{e(p)}$ refers to electrons (protons).

At the critical radius r^* close to the Schwarzschild zone (we argue that $r^* = 1.5r_s$) the decay of quantum statistics takes place due to the topological reason, and both Fermi spheres of electrons and protons collapse. The amount of energy given by Eq. (E2) per one second can be thus released in vicinity of the Schwarzschild zone due to collapse of Fermi spheres. This released energy per second can contribute to the observed luminosity of a quasar (10^{40} W). This undergoes by portions dn of particle flow incoming to an r^* region in infinite small time periods dt , adding up in total to $0.06 \times M_Z$ kg per second. The value of the energy released depends on the local Fermi momentum and attains 10^{40} J at a sufficiently high level of compression, i.e., at sufficiently small $V(r^*)$ determined from the self-consistent system of Eqs. (E1) and (E2) if one assumes $E(r^*) = 10^{40}$ J.

To the initial mass of a gas (assuming to be composed of hydrogen H) contribute mostly protons (ca. 2000 times more massive than electrons), thus the total number of electrons, the same as the number of protons, equals $n \simeq 0.06M_Z/m_p \simeq 2.14 \times 10^{50}$ per second. Simultaneously solving Eqs. (E1) and (E2), assuming $n = 2.14 \times 10^{50}$ in volume $V(r^*)$ and released energy $E(r^*) = 10^{40}$ J, we find the volume of plasma compression $V(r^*) = 0.5 \times 10^5$ m³ and electron or proton Fermi sphere radius $p_F(r^*) = 5.4 \times 10^{-19}$ kg m/s. Electrons and protons (their amount per second) are compressed to the same volume $V(r^*)$ (due to neutrality of plasma), hence, their concentration at r^* , $\rho(r^*) = 4.3 \times 10^{45}$ 1/m³. The mass density at r^* (including mass equivalent to the energy stored up in Fermi spheres of electrons and protons) is thus $\xi(r^*) = \frac{0.06M_Z}{V(r^*)} + \frac{E(r^*)}{c^2 V(r^*)} \simeq 9 \times 10^{18}$ kg/m³, similar to mass density in neutron stars at the Tolman-Oppenheimer-Volkoff limit (being of order of hadron density in atom nuclei). This is the uppermost mass density at the critical r^* , which evidences the self-consistency of the model. This limit regulates the matter

consumption by a black hole, when the supply of the matter to an accretion disk is unlimited in the black hole surroundings. The released energy of $E(r^*) = 10^{40}$ J is equivalent to 30% of the infalling mass of 0.06 Earth mass (per second). It means that the compressed plasma with degenerate Fermi liquid of electrons (and also of protons) is at $r = r^*$ 30% more massive than initial remote diluted gas. This increase of mass is caused by the gravitational field of the central black hole, which compresses both systems of fermions and accumulates the energy in their Fermi spheres.

The energy of the gravitational field is accumulated in Fermi spheres of electrons and protons. The ratio of total Fermi sphere energies of electrons and protons is $\frac{E_e(r^*)}{E_p(r^*)} \simeq 1.4$. The Fermi energy of electrons with Fermi momentum $p_F(r^*) = 5.48 \times 10^{-19}$ kg m/s equals $\varepsilon_F = 1$ GeV (it is the upper possible energy of emitted photons), which in thermal scale (in units of $k_B = 1$) is of order of 10^{13} K; this makes the electron liquid quantumly degenerated at lower temperatures (quasars are not source of thermal gamma radiation, thus their actual temperatures are much lower). The Fermi energy of protons with Fermi momentum $p_F(r^*) = 5.48 \times 10^{-19}$ kg m/s equals $\varepsilon_F = 0.4$ GeV (it is the upper possible energy of emitted photons by jumping of protons), which in the thermal scale (in units of $k_B = 1$) is of order of 4×10^{12} K; thus for the temperature of plasma of order of 10^{6-9} K (the most realistic is 10^6) protons also form the degenerated Fermi liquid.

The release of energy due to the collapse of the Fermi sphere of charged particles undergoes according to the Fermi golden rule scheme for quantum transitions [52], when such transitions are admitted by the local revoking of the Pauli exclusion principle. Charged carries (electrons and protons) couple to the electromagnetic field, and the matrix element of this coupling between an individual particle state in the Fermi sphere and its ground state is the kernel of the Fermi golden rule formula for transition probability per time unit for this particle. This interaction depends also on electromagnetic field strength, thus the increasing number of excited photons strengthens the coupling in the similar manner as at stimulated emission (known from, e.g., laser action) and accelerates quantum transition of the Fermi sphere collapse.

Note that the above estimation of the energy accumulated in Fermi spheres at the critical distance from the gravitational singularity has been done in conventional rigid coordinates, time and space-spherical coordinates (t, r, θ, ϕ) of the remote observer. The Schwarzschild metric (15), though written in the rigid and stationary coordinates, describes the folded spacetime. Even if in Eq. (E1) one replaces $V(r)$ by the proper volume at the distance r from the central singularity, then according to the Schwarzschild metric (15) one obtains for the elementary proper volume the formula

$$dV = \left(1 - \frac{r_s}{r}\right)^{-1/2} dr r^2 \sin\theta d\theta d\phi, \quad (\text{E3})$$

which is only by the factor $(1 - \frac{r_s}{r})^{-1/2}$ greater than $dV = dr r^2 \sin\theta d\theta d\phi$ in the remote observer coordinates neglecting curvature. At $r^* = 1.5r_s$ this factor is ca. 1.7, which gives the reduction of p_F caused by gravitation curvature by a factor ca. $1.7^{-1/3} \simeq 0.84$, which does not change orders in the above

estimations. The change of p_F by one order of magnitude would need the closer approaching the Schwarzschild horizon, at $r \simeq 1.000001r_s$, i.e., rather distant from the critical $r^* = 1.5r_s$. Hence, for the rough estimation of the effect of

Fermi sphere collapse the correction (E3) is unimportant and can be included as the factor 0.84 to the right-hand side of Eq. (E1), which does not change the orders in the energy estimation.

-
- [1] R. P. Feynman and A. R. Hibbs, *Quantum Mechanics and Path Integrals* (McGraw-Hill, New York, 1964).
- [2] M. Chaichian and A. Demichev, *Path Integrals in Physics, Volume I, Stochastic Processes and Quantum Mechanics* (IOP Publishing, Bristol, 2001).
- [3] M. Chaichian and A. Demichev, *Path Integrals in Physics, Volume II, Quantum Field Theory, Statistical Physics and Other Modern Applications* (IOP Publishing, Bristol, 2001).
- [4] E. Spanier, *Algebraic Topology* (Springer-Verlag, Berlin, 1966).
- [5] N. D. Mermin, The topological theory of defects in ordered media, *Rev. Mod. Phys.* **51**, 591 (1979).
- [6] N. Wiener, The average of an analytic functional, *Proc. Natl. Acad. Sci. USA* **7**, 253 (1921).
- [7] W. Pauli, *Pauli Lectures on Physics*, Vol. 6 (MIT Press, Cambridge, MA, 1973), Chap. 7.
- [8] R. D. Nevels, Z. Wu, and C. Huang, Feynman path integral for an infinite potential barrier, *Phys. Rev. A* **48**, 3445 (1993).
- [9] J. S. Birman, *Braids, Links and Mapping Class Groups* (Princeton University Press, Princeton, 1974).
- [10] E. Artin, Theory of braids, *Ann. Math.* **48**, 101 (1947).
- [11] M. G. Laidlaw and C. M. DeWitt, Feynman functional integrals for systems of indistinguishable particles, *Phys. Rev. D* **3**, 1375 (1971).
- [12] E. C. G. Sudarshan, T. D. Imbo, and T. R. Govindarajan, Configuration space topology and quantum internal symmetries, *Phys. Lett. B* **213**, 471 (1988).
- [13] Y. S. Wu, General Theory for Quantum Statistics in Two Dimensions, *Phys. Rev. Lett.* **52**, 2103 (1984).
- [14] T. D. Imbo, C. S. Imbo, and C. S. Sudarshan, Identical particles, exotic statistics and braid groups, *Phys. Lett. B* **234**, 103 (1990).
- [15] F. Wilczek, *Fractional Statistics and Anyon Superconductivity* (World Scientific, Singapore, 1990).
- [16] N. Ashcroft and D. Mermin, *Solid State Physics* (Holt, Rinehart & Winston, New York, 1976).
- [17] J. R. Klauder and E. Onorfi, Landau levels and geometric quantization, *Int. J. Mod. Phys. A* **04**, 3939 (1989).
- [18] J. R. Klauder, Quantization is geometry, after all, *Ann. Phys.* **188**, 120 (1988).
- [19] K. v. Klitzing, G. Dorda, and M. Pepper, New Method for High-Accuracy Determination of the Fine-Structure Constant Based on Quantized Hall Resistance, *Phys. Rev. Lett.* **45**, 494 (1980).
- [20] D. C. Tsui, H. L. Störmer, and A. C. Gossard, Two-Dimensional Magnetotransport in the Extreme Quantum Limit, *Phys. Rev. Lett.* **48**, 1559 (1982).
- [21] J. E. Jacak, Topological approach to electron correlations at fractional quantum Hall effect, *Ann. Phys.* **430**, 168493 (2021).
- [22] R. E. Prange and S. M. Girvin, *The Quantum Hall Effect* (Springer Verlag, New York, 1990).
- [23] O. Ciftja and C. Wexler, Monte Carlo simulation method for Laughlin-like states in a disk geometry, *Phys. Rev. B* **67**, 075304 (2003).
- [24] R. Morf and B. I. Halperin, Monte carlo evaluation of trial wavefunctions for the fractional quantized Hall effect: Spherical geometry, *Z. Phys. B Condensed Matter* **68**, 391 (1987).
- [25] W. Pan, H. L. Störmer, D. C. Tsui, L. N. Pfeiffer, K. W. Baldwin, and K. W. West, Fractional Quantum Hall Effect of Composite Fermions, *Phys. Rev. Lett.* **90**, 016801 (2003).
- [26] R. B. Laughlin, Anomalous Quantum Hall Effect: An Incompressible Quantum Fluid with Fractionally Charged Excitations, *Phys. Rev. Lett.* **50**, 1395 (1983).
- [27] F. D. M. Haldane, Fractional Quantization of the Hall Effect: A Hierarchy of Incompressible Quantum Fluid States, *Phys. Rev. Lett.* **51**, 605 (1983).
- [28] B. I. Halperin, Statistics of Quasiparticles and the Hierarchy of Fractional Quantized Hall States, *Phys. Rev. Lett.* **52**, 1583 (1984).
- [29] J. K. Jain, Composite-Fermion Approach for the Fractional Quantum Hall Effect, *Phys. Rev. Lett.* **63**, 199 (1989).
- [30] B. I. Halperin, Theory of the quantized Hall conductance, *Helv. Phys. Acta* **56**, 75 (1983).
- [31] J. K. Jain, *Composite Fermions* (Cambridge University Press, Cambridge, 2007).
- [32] J. E. Jacak, Application of the path integral quantization to indistinguishable particle systems topologically confined by a magnetic field, *Phys. Rev. A* **97**, 012108 (2018).
- [33] J. E. Jacak, Formal derivation of the Laughlin function and its generalization for other topological phases of FQHE, *Sci. Rep.* **12**, 616 (2022).
- [34] J. Jacak, Unconventional fractional quantum Hall effect in bilayer graphene, *Sci. Rep.* **7**, 8720 (2017).
- [35] C. R. Dean, A. F. Young, P. Cadden-Zimansky, L. Wang, H. Ren, K. Watanabe, T. Taniguchi, P. Kim, J. Hone, and K. L. Shepard, Multicomponent fractional quantum Hall effect in graphene, *Nat. Phys.* **7**, 693 (2011).
- [36] F. Amet, A. J. Bestwick, J. R. Williams, L. Balicas, K. Watanabe, T. Taniguchi, and D. Goldhaber-Gordon, Composite fermions and broken symmetries in graphene, *Nat. Commun.* **6**, 5838 (2015).
- [37] D. K. Ki, V. I. Falko, D. A. Abanin, and A. Morpurgo, Observation of even denominator fractional quantum Hall effect in suspended bilayer graphene, *Nano Lett.* **14**, 2135 (2014).
- [38] J. Jacak and L. Jacak, The commensurability condition and fractional quantum Hall effect hierarchy in higher Landau levels, *JETP Lett.* **102**, 19 (2015).
- [39] G. Diankov, C.-T. Liang, F. Amet, P. Gallagher, M. Lee, A. J. Bestwick, K. Tharratt, W. Coniglio, J. Jaroszynski, K. Watanabe *et al.*, Robust fractional quantum Hall effect in the $N = 2$ Landau level in bilayer graphene, *Nat. Commun.* **7**, 13908 (2016).

- [40] P. Maher, L. Wang, Y. Gao, C. Forsythe, T. Taniguchi, L. Watanabe, D. Abanin, Z. Papić, P. Cadden-Zimansk, J. Hone *et al.*, Tunable fractional quantum Hall phases in bilayer graphene, *Science* **345**, 61 (2014).
- [41] K. Schwarzschild, Über das Gravitationsfeld eines Massenpunktes nach der Einsteinschen Theorie, *Sitzungsber. Preuss. Akad. Wiss. Berlin (Math. Phys.)* **1916**, 189 (1916).
- [42] I. D. Novikov and K. S. Thorne, *Black Holes (Les Astres Occlus) by C. DeWitt and B. S. DeWitt* (Gordon and Breach Science Publishers, London, 1973).
- [43] M. D. Kruskal, Maximal extension of Schwarzschild metric, *Phys. Rev.* **119**, 1743 (1960).
- [44] G. Szekeres, On the singularities of a Riemannian manifold, *Publ. Math. Debrecen* **7**, 285 (1960).
- [45] W. Pauli, The connection between spin and statistics, *Phys. Rev.* **58**, 716 (1940).
- [46] S. Chandrasekhar, The maximum mass of ideal white dwarfs, *Astrophys. J.* **74**, 81 (1931).
- [47] R. C. Tolman, Static solutions of Einstein's field equations for spheres of fluid, *Phys. Rev.* **55**, 364 (1939).
- [48] J. R. Oppenheimer and G. M. Volkoff, On massive neutron cores, *Phys. Rev.* **55**, 374 (1939).
- [49] D. G. Yakovlev, P. Haensel, G. Baym, and C. Pethick, Lev Landau and the concept of neutron stars, *Phys.-Usp.* **56**, 289 (2013).
- [50] A. A. Abrikosov, L. P. Gorkov, and I. E. Dzialoshinskii, *Methods of Quantum Field Theory in Statistical Physics* (Dover Publications, Mineola, NY, 1975).
- [51] J. M. Luttinger, Fermi surface and some simple equilibrium properties of a system of interacting fermions, *Phys. Rev.* **119**, 1153 (1960).
- [52] L. D. Landau and E. M. Lifshitz, *Quantum Mechanics: Non-relativistic Theory* (Nauka, Moscow, 1972).
- [53] S. W. Hawking, Black hole explosions? *Nature (London)* **248**, 30 (1974).
- [54] A. Bekenstein, Black holes and the second law, *Lett. Nuovo Cimento* **4**, 737 (1972).
- [55] W. G. Unruh, Notes on black-hole evaporation, *Phys. Rev. D* **14**, 870 (1976).
- [56] S. W. Hawking, Breakdown of predictability in gravitational collapse, *Phys. Rev. D* **14**, 2460 (1976).
- [57] A. Almheiri, D. Marolf, J. Polchinski, and J. Sully, Black holes: Complementarity or firewalls? *J. High Energy Phys.* **02** (2013) 062.
- [58] A. Almheiri, T. Hartman, J. Maldacena, E. Shaghoulian, and A. Tajdini, The entropy of Hawking radiation, *Rev. Mod. Phys.* **93**, 035002 (2021).
- [59] N. I. Shakura and R. A. Sunyaev, Black holes in binary systems. Observational appearance, *Astron. Astrophys.* **24**, 337 (1973).
- [60] E. E. Salpeter, Accretion of interstellar matter by massive objects, *Astrophys. J.* **140**, 796 (1964).
- [61] Ya. B. Zel'dovich, The fate of a star, and the liberation of gravitation energy in accretion, *Dokl. Akad. Nauk SSSR* **155**, 67 (1964).
- [62] J. Frank, A. King, and D. Derek, *Accretion Power in Astrophysics*, 3rd ed. (Cambridge University Press, Cambridge, 2002).
- [63] A. Merloni, A. C. Fabian, and R. R. Ross, On the interpretation of the multicolour disc model for black hole candidates, *Mon. Not. R. Astron. Soc.* **313**, 193 (2000).
- [64] S. L. Shapiro, A. P. Lightman, and D. M. Eardley, A two-temperature accretion disk model for Cygnus X-1: Structure and spectrum, *Astrophys. J.* **204**, 187 (1976).
- [65] M. Brightman, M. Bachetti, H. P. Earnshaw, F. Fürst, J. García, B. Grefenstette, M. Heida, E. Kara, K. K. Madsen, M. J. Middleton *et al.*, Breaking the limit: Super-Eddington accretion onto black holes and neutron stars, *Bull. Am. Astronom. Soc.* **51**, 352 (2019).
- [66] P. C. Fragile, S. M. Etheridge, P. Anninos, B. Mishra, and W. Kluźniak, Relativistic, viscous, radiation hydrodynamic simulations of geometrically thin disks. I. Thermal and other instabilities, *Astronom. J.* **857**, 1 (2018).
- [67] D. Farrah, A. Efstathiou, J. Afonso, J. Bernard-Salas, J. Cairns, D. Clements, K. Croker, E. Hatziminaoglou, M. Joyce, M. Lacy *et al.*, Stellar and black hole assembly in $z < 0.3$ infrared-luminous mergers: intermittent starbursts vs. super-Eddington accretion, *Mon. Not. R. Astron. Soc.* **513**, 4770 (2022).
- [68] J. Dexter, N. Scepi, and M. C. Begelman, Radiation GRMHD simulations of the hard state of black hole x-ray binaries and the collapse of a hot accretion flow, *Astrophys. J. Lett.* **919**, L20 (2021).
- [69] S. Laha, E. Meyer, A. Roychowdhury, J. Becerra Gonzalez, J. A. Acosta-Pulido, A. Thapa, R. Ghosh, E. Behar, L. C. Gallo, G. A. Kriss *et al.*, A radio, optical, UV, and X-ray view of the enigmatic changing-look active galactic nucleus IES 1927+654 from its pre- to postflare states, *Astrophys. J.* **931**, 5 (2022).
- [70] R. D. Blandford and R. L. Znajek, Electromagnetic extraction of energy from Kerr black holes, *Mon. Not. R. Astron. Soc.* **179**, 433 (1977).
- [71] M. O. Goerbig, Electronic properties of graphene in a strong magnetic field, *Rev. Mod. Phys.* **83**, 1193 (2011).
- [72] L. D. Landau and E. M. Lifshitz, *Field Theory* (Fizmatlit, Moscow, 2001).
- [73] L. D. Landau and E. M. Lifshitz, *Short Course of Theoretical Physics: Quantum Mechanics* (Nauka, Moscow, 1978).
- [74] I. Duck and E. C. G. Sudarshan, Toward an understanding of the spin-statistics theorem, *Am. J. Phys.* **66**, 284 (1998).
- [75] I. Duck and E. C. G. Sudarshan, *Pauli and the Spin-Statistics Theorem* (World Scientific, Singapore, 1997).
- [76] J. M. Leinaas and J. Myrheim, On the theory of identical particles, *Nuovo Cimento B* **37**, 1 (1977).
- [77] Y. R. Rumer and A. I. Fet, *Theory of Unitary Symmetry* (Nauka, Moscow, 1970).